

# Scenarios of domain pattern formation in a reaction-diffusion system

C. B. Muratov

*Department of Physics, Boston University, Boston, Massachusetts 02215*

V. V. Osipov

*Department of Theoretical Physics, Russian Science Center  
"Orion"*

*2/46 Plekhanov St., Moscow 111123, Russia*

(November 20, 2018)

We performed an extensive numerical study of a two-dimensional reaction-diffusion system of the activator-inhibitor type in which domain patterns can form. We showed that both multidomain and labyrinthine patterns may form spontaneously as a result of Turing instability. In the stable homogeneous system with the fast inhibitor one can excite both localized and extended patterns by applying a localized stimulus. Depending on the parameters and the excitation level of the system stripes, spots, wriggled stripes, or labyrinthine patterns form. The labyrinthine patterns may be both connected and disconnected. In the stable homogeneous system with the slow inhibitor one can excite self-replicating spots, breathing patterns, autowaves and turbulence. The parameter regions in which different types of patterns are realized are explained on the basis of the asymptotic theory of instabilities for patterns with sharp interfaces developed by us in *Phys. Rev. E* **53**, 3101 (1996). The dynamics of the patterns observed in our simulations is very similar to that of the patterns forming in the ferrocyanide-iodate-sulfite reaction.

PACS number(s): 05.70.Ln, 82.20.Mj, 47.54.+r

## I. INTRODUCTION

Pattern formation and self-organization are among the most fascinating phenomena in modern science that are observed in physical, chemical, and biological systems of very different nature (for the books and recent reviews on this subject see [1–13], where a lot of references to the original works can also be found). As a rule, self-organization is associated with Turing instability of the homogeneous state in the nonequilibrium systems and spontaneous formation of patterns (dissipative structures) in them as the excitation level of the system (or some other parameter) is varied [1–8,10,12]. At the same time, when the homogeneous state of such a system is stable, by applying a sufficiently strong perturbation one can excite static, pulsating, and traveling patterns including solitary patterns — autosolitons (AS) [9,11–14].

Consider, for example, chemical patterns forming in the ferrocyanide-iodate-sulfite (FIS) reaction in a gel reactor [15–17]. In a typical experimental setting a pattern may form spontaneously as a result of the instability of the homogeneous state or can be excited by a short localized external perturbation of the system. The patterns forming in both these cases do not have any qualitative differences. They are essentially the domains of high and low concentrations of certain substance separated by relatively sharp walls. The pattern may have sophisticated geometry and in general may show very complicated spatio-temporal behavior. The properties of the patterns do not significantly depend on whether the system is monostable or bistable.

It appears that domain patterns forming in very dif-

ferent systems may in fact have many common features. This has recently been noticed in the case of static domain patterns forming both in equilibrium and nonequilibrium systems, where a certain set of domain shapes, such as spots, stripes, multidomain and labyrinthine patterns, and the transitions between them has been observed [18]. The same conclusion can be extended to the dynamic patterns in nonequilibrium systems. Indeed, traveling, pulsating, self-replicating, and stochastically oscillating patterns are observed in the systems as diverse as autocatalytic reactions [8,15–17], semiconductor and gas plasma [10–14,19], or premixed flames [20–22]. All this suggests that there exists a universality class of the nonequilibrium systems in which pattern formation and self-organization scenarios are essentially the same.

Another important question raised by the experiments is to identify the totality of possible types of patterns and their behaviors in the systems under consideration, and to understand the requirements the system should meet in order to be able to produce one type of pattern or the other.

In the present paper we will study a model which is a typical representative of the pattern-forming systems whose phenomenology was discussed above. We will show that the type of patterns that form in this model is determined mainly by the relationship between the characteristic length and time scales of the systems and the way the system is excited. We will also show that by changing only these length and time scales and choosing an appropriate form for the external stimulus one can make the system form practically all kinds of patterns, both static and dynamic, that are observed in the experiments.

Our paper is organized as follows: in Sec. II we discuss the physical mechanisms of pattern formation phenomena in reaction-diffusion systems of the activator-inhibitor type, using a combustion model as an example, and introduce a simple model which we study numerically; in Sec. III we present the results of a systematic numerical study of the reaction-diffusion model and give qualitative explanations to the effects seen; in Sec IV we use the general asymptotic theory of instabilities developed by us in Ref. [23] to identify the parameter regions in which one or the other type of patterns is observed and compare these regions with the results of the simulations, we also give more substantial quantitative explanations for the pattern behaviors that are observed basing on the interfacial dynamics approach; and finally, in Sec. V we compare our results with various experiments and draw conclusions.

## II. THE MODEL

The model which describes the phenomenology of pattern formation in many nonequilibrium systems is a pair of reaction-diffusion systems of the activator-inhibitor type

$$\tau_\theta \frac{\partial \theta}{\partial t} = l^2 \Delta \theta - q(\theta, \eta, A), \quad (1)$$

$$\tau_\eta \frac{\partial \eta}{\partial t} = L^2 \Delta \eta - Q(\theta, \eta, A), \quad (2)$$

where  $\theta$  is the activator,  $\eta$  is the inhibitor,  $l$  and  $L$  are the characteristic length scales, and  $\tau_\theta$  and  $\tau_\eta$  are the characteristic time scales of the activator and the inhibitor, respectively,  $q$  and  $Q$  are certain non-linear functions, and  $A$  is the bifurcation parameter. Equations (1) and (2) have been extensively used to study pattern formation in various nonequilibrium systems. In particular, they describe electron-hole and gas plasma, various semiconductor, superconductor, and gas-discharge structures, systems with uniformly generated combustion material [10–14]; chemical reactions with autocatalysis and cross-catalysis [2,6,8]; models of morphogenesis and population dynamics in biology [4]. Some systems with phase transitions, such as diblock copolymer blends and ferroelectric semiconductors, are also described by equations which can be reduced to Eqs. (1) and (2) [24–26].

Pattern formation in the systems under consideration is associated with a positive feedback of the activator  $\theta$  which results in “self-production of the activator substance”, this process of self-production is controlled by the inhibitor  $\eta$  that suppresses the growth of the activator. It is these two competing processes that give rise to different kinds of patterns in these systems.

The meaning of the variables  $\theta$  and  $\eta$  can be most easily understood for the system with uniformly generated

combustion material [11,12]. Consider combustion process in the flow reactor consisting of a chamber placed between the two porous slabs which are being cooled. The mixture of fuel and oxidizer is pumped through the narrow reactor region between the slabs where it is ignited. Phenomenologically, this system may be described by the equations for the mass diffusion and the heat conductance which include the reaction terms, averaged over the thickness of the reactor region. If  $n$  is the concentration of the fuel and  $T$  is the temperature of the mixture, these equations have the form:

$$\frac{\partial n}{\partial t} = D \Delta n + G(n) - R(n, T), \quad (3)$$

$$c\rho \frac{\partial T}{\partial t} = \kappa \Delta T + ER(n, T) - W(T), \quad (4)$$

where  $G = (n_0 - n)/\tau_n$  is the rate of the fuel supply,  $R(n, T) = \alpha n \exp(-E_a/T)$  is the reaction rate,  $E_a$  is the activation energy,  $E$  is the reaction heat and  $\alpha$  is a coefficient;  $W(T) = c\rho(T - T_0)/\tau_T$  is the heat removed from the mixture,  $\rho$  is the density,  $c$  is the heat capacity of the mixture,  $T_0$  is the temperature of the environment;  $D$  and  $\kappa$  are the diffusivity and the thermal conductivity, respectively,  $\tau_n$  and  $\tau_T$  are time constants, and  $\Delta$  is the two-dimensional Laplacian. In this system the activator is the temperature  $T$ , and the inhibitor is the concentration  $n$ . Suppose that the system is initially in the low-temperature state. Now, if a localized region of the mixture is heated up, the rate of the reaction in that region will rapidly increase, thus producing more heat and igniting the neighboring areas. However, this process cannot go forever, since as the reaction proceeds, the fuel is being used up, which in turn decreases the rate of the reaction. Thus, a positive feedback is realized with respect to the temperature and the negative feedback with respect to the concentration. If we introduce the variables  $\theta = T/E_a$ ,  $\eta = n/n_0$ ,  $l = \sqrt{\kappa\tau_T/c\rho}$ ,  $L = \sqrt{D\tau_n}$ , and  $A = \alpha n_0 E \tau_T / c\rho E_a$ , we will arrive at Eqs. (1) and (2).

Pattern formation is most pronounced in chemical and biological systems [1–6,8,15–17] where the processes of self-production of matter are responsible for it. However, in the real situation such systems are extremely complicated. Nevertheless, it is often possible to reduce the description of these systems to a pair of reaction-diffusion equations of the activator-inhibitor type [1–6,8]. A particularly simple model of this kind is the “cubic” model, which is described by Eqs. (1) and (2) with

$$q = \theta^3 - \theta - \eta, \quad (5)$$

$$Q = \theta + \eta - A. \quad (6)$$

This model will be studied numerically and analytically in the subsequent sections.

Kerner and Osipov showed that the properties of the patterns and pattern formation scenarios in the systems

described by Eqs. (1) and (2) are chiefly determined by the parameters  $\epsilon = l/L$  and  $\alpha = \tau_\theta/\tau_\eta$ , and the shape of the nullcline of Eq. (1) for the activator [10–12]. In many cases, including the cubic model and the model described by Eqs. (3) and (4), this nullcline is N-shaped (see Fig. 1). In these systems static, pulsating, and traveling patterns may form at different values of the parameters  $\epsilon$  and  $\alpha$ .

When  $\alpha \ll 1$  and  $\epsilon \gtrsim 1$ , that is when the inhibitor is slower and shorter-ranged than the activator, only traveling patterns may exist. In the limit  $\epsilon \rightarrow \infty$  (or, more precisely, for  $L = 0$ ) the properties of such traveling patterns were studied in detail in both one-dimensional and higher-dimensional cases (see, for example, [2,3,5,8] and references therein). In the other limiting case  $\epsilon \ll 1$  and  $\alpha \gtrsim 1$ , that is when the inhibitor is long-range and fast compared to the activator, only static patterns may form [10–12]. These patterns are essentially the domains of high and low activator values separated by the narrow walls (interfaces) whose width is of order  $l$ . Traveling, static, and pulsating domain patterns may form when both  $\epsilon \ll 1$  and  $\alpha \ll 1$ .

Let us elucidate the physics of the formation of static, traveling, and pulsating patterns, including the simplest patterns — AS (Fig. 2), using the combustion system described by Eqs. (3) and (4). First of all, it is clear that if both the characteristic time and length scales of the variation of the concentration  $n$  are much smaller than the characteristic scales of the variation of the temperature  $T$ , no patterns will form. Indeed, if a localized region of the system is ignited, all the fuel will burn down very fast in that region and the flame will not be able to propagate, so after a short time after removing the heat source the flame will extinguish. Different situation is realized if the diffusivity of the fuel is much smaller than the thermal diffusivity and the characteristic time scale of the temperature relaxation  $\tau_T$  due to the heat exchange between the mixture and the porous slabs is much longer than the characteristic time scale  $\tau_n$  of the concentration variation determined by the rate of the fuel supply. Then the conditions  $\alpha \ll 1$  and  $\epsilon \gtrsim 1$  may be satisfied and the patterns in the form of traveling flames may be excited in the system. The existence of traveling patterns is due to the fact that because of high heat conductance the region of size of order  $l = \sqrt{\kappa\tau_T/c\rho}$  around the flame is heated up and ignited. As a result, the released heat ignites the neighborhood and so on. This leads to the formation of a flame front moving with the speed  $v \simeq l/\tau_T$  [Fig. 2(a)]. The fuel after the front burns down, so the front is followed by the back separated from the front by the distance of order  $v\tau_n \gg l$ . Because of the external supply the fuel replenishes at the distances of order  $v\tau_n$  away from the back.

If the diffusivity of the fuel is much larger than the thermal diffusivity of the mixture, the condition  $\epsilon \ll 1$  and  $\alpha \gtrsim 1$  may be satisfied. Then a traveling flame front will stop since high diffusion of the fuel will result in the decrease of the fuel concentration ahead of the front and

lead to the formation of the static pattern in the form of a flame cell [Fig. 2(b)]. The existence of such static pattern is due to the fact that the flame is maintained by the diffusive influx of the fuel from the neighborhood, where it is constantly supplied through the porous slabs. It is clear that when both  $\epsilon \ll 1$  and  $\alpha \ll 1$ , pulsating flames, or more complex dynamic patterns, may form in the system [Fig. 2(c)]. The cell may first expand, but as it cools down and the fuel is used up in it, the front may stop and start traveling back [11,12].

From the physical considerations above follows that in order for patterns to be able to form, either  $\epsilon$  or  $\alpha$  has to be small. Kerner and Osipov suggested the classification scheme for the reaction-diffusion systems of the activator-inhibitor type based on the relationship between the values of  $\epsilon$  and  $\alpha$  [9–12]. According to this scheme, a system with N-shaped nullcline of the equation for the activator is called  $\Omega N$  system if  $\alpha \ll 1$  and  $\epsilon \gtrsim 1$ ;  $KN$  system, if  $\epsilon \ll 1$  and  $\alpha \gtrsim 1$ ; or  $K\Omega N$  systems, if both  $\alpha \ll 1$  and  $\epsilon \ll 1$ . Accordingly, only traveling waves (autowaves) may form in  $\Omega N$  systems, only static patterns in  $KN$  systems, and all kinds of patterns in  $K\Omega N$  systems.

Clearly, the mechanisms of pattern formation in all reaction-diffusion systems described by Eqs. (1) and (2) are essentially the same as those discussed above. For example, similar processes lead to the formation of static, traveling, and pulsating patterns in the form of the regions of high temperature and low concentration of electrons in the photo-generated electron-hole plasma heated in the process of Auger recombination [11,12,27]. For this reason we may use the simple “cubic” model described by Eqs. (1) and (2) with (5) and (6) in all our numerical simulations. Depending on  $\alpha$  and  $\epsilon$ , this system will pertain to one of the three classes mentioned above. In this paper we will concentrate on the case when the system under consideration is either  $KN$  or  $K\Omega N$  system.

### III. SCENARIOS OF PATTERN FORMATION: RESULTS OF THE SIMULATIONS

If we choose  $L$  and  $\tau_\eta$  as the units of length and time, respectively, we will write the equations describing the cubic model in the form

$$\alpha \frac{\partial \theta}{\partial t} = \epsilon^2 \Delta \theta - \theta^3 + \theta + \eta, \quad (7)$$

$$\frac{\partial \eta}{\partial t} = \Delta \eta - \theta - \eta + A. \quad (8)$$

We performed numerical simulations of Eqs. (7) and (8) in two dimensions in a wide range of the parameters  $\epsilon$ ,  $\alpha$ , and  $A$ . As we mentioned earlier, either  $\epsilon$  or  $\alpha$  has to be small in order for patterns to be able to form. The case of  $\Omega N$  systems was extensively studied by many authors [2,3,5,8] and will not be studied here. We will concentrate on the case  $\epsilon \ll 1$  and arbitrary  $\alpha$ .

The presence of two very different length scales caused by the smallness of the parameter  $\epsilon$  makes the numerical simulations of Eqs. (7) and (8) rather difficult. The simulations were performed on the massively parallel supercomputer. An explicit second order finite difference scheme was used to discretize the equations. In order to accelerate the algorithm, different grid spacings were used for  $\theta$  and  $\eta$ . The boundary conditions were neutral or periodic. The grid spacing was chosen in such a way that a typical front of a pattern contained about 8 to 10 points. The decrease of the grid spacing by a factor of two resulted in the difference of the distributions of  $\theta$  and  $\eta$  by a few percent. No noticeable effects on the dynamics were observed.

Before discussing the results of the simulations, let us make a few comments about the system of Eqs. (7) and (8). First of all, it is easy to see that these equations are invariant with respect to the transformation

$$\theta \rightarrow -\theta, \quad \eta \rightarrow -\eta, \quad A \rightarrow -A, \quad (9)$$

so one only needs to study the parameter region where  $A < 0$ . The system under consideration is monostable for all values of  $A$ . The homogeneous state  $\theta = \theta_h$  and  $\eta = \eta_h$  with

$$\theta_h = -|A|^{1/3}, \quad \eta_h = |A|^{1/3}(1 - |A|^{2/3}) \quad (10)$$

is stable for  $A < A_0 = -1/3\sqrt{3} \simeq -0.19$ , where  $A_0$  is the value of  $A$  at which  $\theta_h = \theta_0$  and  $\eta_h = \eta_0$ , the point on the nullcline of Eq. (7) at which  $q'_\theta = 0$  (see Fig. 1). It is easy to see [9–12] that for  $\alpha < 1$  the homogeneous state becomes unstable with respect to the uniform oscillations (Hopf bifurcation) with the frequency

$$\omega_0 = \left(\frac{1-\alpha}{\alpha}\right)^{1/2} \quad \text{at } A > A_\omega = -\left(\frac{1-\alpha}{3}\right)^{3/2}, \quad (11)$$

whereas for  $\epsilon < 1$  it destabilizes with respect to the fluctuations with the wave vector  $k = k_0$  and zero frequency (Turing bifurcation)

$$k_0 = \left(\frac{1-\epsilon}{\epsilon}\right)^{1/2} \quad \text{at } A > A_c = -\left(\frac{1-\epsilon}{\sqrt{3}}\right)^3. \quad (12)$$

Notice that for  $\epsilon \rightarrow 0$  or  $\alpha \rightarrow 0$  we have  $A_c \rightarrow A_0$  or  $A_\omega \rightarrow A_0$ , respectively. Also notice that the homogeneous state is always stable when  $\epsilon > 1$  and  $\alpha > 1$ . It is the considerations of stability of the homogeneous state that actually lead Kerner and Osipov to divide the system described by Eqs. (1) and (2) into  $\Omega N$ ,  $KN$ , and  $K\Omega N$  systems [10–12]. Similar classification of pattern-forming systems of different nature, including the hydrodynamic systems, was proposed later by Cross and Hohenberg [7].

Most of our simulations were performed at  $\epsilon = 0.05$ , what can be considered reasonably small. In the first simulations we studied the Turing instability. The boundary

conditions in these simulations were periodic. The initial condition was taken in the form of the homogeneous state plus small random noise. The system then evolved for a considerably long time at  $A = -0.1$  and  $\alpha = 0.5$  when the homogeneous state is unstable with respect to Turing instability but stable with respect to the oscillatory instability. The process of formation of static Turing pattern is shown in Fig. 3. In the early stage ( $t = 6$  and  $t = 9$  in Fig. 3) the system nucleates some random distribution of the activator and the inhibitor. At the intermediate stage ( $t = 16$ ) the pattern transforms into a number of domains with sharp walls, at this point the domains may have irregular shapes and domain fusion frequently occurs; at the late stage ( $t = 51$  and  $t = 210$ ) the domains rearrange so that their shape becomes more regular, and a lot of smaller domains die through overcrowding. One can see that in the end the static Turing (multidomain) pattern consists of many disconnected domains with sharp walls. Most of them look like slightly distorted circular domains of different sizes, although some are more stripe-like. The pattern is metastable, upon longer runs a small portion of domains may occasionally disappear or change their geometry, but its overall appearance remains the same. The interaction between the neighboring domains appears to be repulsive, so one should expect an ideal hexagonal pattern of circular domains of certain radius to be the most stable one. This pattern reminds of the ordered cellular flame pattern observed in the combustion experiments [20] and ordered pattern of current filaments in the gas-discharge experiments [19].

In the next simulation the initial condition is taken the same, but the parameters now are  $A = -0.1$  and  $\alpha = 0.05$ , so that the homogeneous state is unstable both with respect to the Turing instability and the oscillatory instability. The evolution of the system toward the static labyrinthine pattern in this case is shown in Fig. 4. The early stage of the formation of the pattern ( $t = 0.6$  and  $t = 0.9$ ) is the same as in the previous case, but once the domains form they start to oscillate (breathe), so the high activator value domains invade almost all the space in the time interval from  $t = 1.2$  to  $t = 2.1$ , but then recede, and the process continues. For this value of  $\alpha$  the pattern finally stabilizes, and eventually a static labyrinthine pattern forms. Notice that both the multidomain pattern which formed at  $t = 955$  in Fig. 3 and the labyrinthine pattern which formed at  $t = 9.2$  in Fig. 4 are perfectly good Turing patterns formed as a result of Turing instability, so there is no qualitative difference between the two. The form of the Turing pattern in any particular situation must therefore depend on the history of getting the homogeneous system into the unstable state. The form of the Turing pattern may also strongly depend on the small local inhomogeneities always present in real systems [10–12]. Notice that both the multidomain and labyrinthine Turing patterns were observed in chemical experiments [6,8,17].

Our simulations show that for sufficiently small  $\alpha$  the uniform self-oscillations of the homogeneous state will all

ways set in upon the destabilization of the homogeneous state even if the system is unstable with respect to the Turing instability. Specifically, for  $\epsilon = 0.05$  this will happen, if  $\alpha < 0.02$ . For larger values of  $\alpha$  the static Turing pattern will always form, although the oscillations of the pattern may last a long time.

In the next series of the simulations we investigate the formation of patterns when the homogeneous state of the system is stable. In all these simulations the boundary conditions were neutral.

It is well known that when  $\alpha \ll 1$  and  $\epsilon \gtrsim 1$  ( $\Omega N$  systems) Eqs. (1) and (2) admit solutions only in the form of traveling waves (autowaves) [2,3,5,8,10,12,28,29], and when  $\epsilon \ll 1$  and  $\alpha \gtrsim 1$  (KN systems) they admit only solutions in the form of static patterns, the simplest of which are AS in the form of solitary spots and stripes of high or low values of the activator surrounded by the “sea” of low or high values of the activator, respectively (“hot” and “cold” AS) [11,12]. Notice that because of the monostability of the considered system the radius of a spot or the width of a stripe cannot be greater than certain value of order one [11,12]. Also note that because of the symmetry given by Eq. (9), in the system under consideration we only need to consider the behavior of hot patterns.

When the homogeneous state of the systems is stable, the patterns may be excited by means of sufficiently strong external stimulus [11,12]. According to the general qualitative theory, the excitation level  $A$  of the system must be greater than certain threshold value  $A_b$  in order for AS to be able to form [10–12]. It is possible to show that in the limit  $\epsilon \rightarrow 0$  the value of  $A_b = -1$  in the considered system.

First we will consider KN systems. Our numerical simulations show that when  $A$  is close to  $A_b$ , the initial condition in the form of the homogeneous state plus a hot spot of size of order several  $\epsilon$  evolves into an AS in the form of a localized static radially-symmetric spot. For  $\epsilon = 0.05$  this happens if  $A_b^{(2)} < A < A_{c2}^{(2)}$ , where  $A_b^{(2)} \simeq -0.72$  and  $A_{c2}^{(2)} \simeq -0.55$ . If the initial condition is taken in the form of the homogeneous state plus a hot stripe several  $\epsilon$  wide, it will evolve into a static stripe if  $A_b^{(1)} < A < A_{c2}^{(1)}$ , where  $A_b^{(1)} \simeq -0.74$  and  $A_{c2}^{(1)} \simeq -0.55$  (the value of  $A_{c2}^{(1)}$  obtained from the simulations is rather crude since the destabilization of the stripe may be incredibly slow).

If the value of  $A$  is increased from  $A_b^{(2)}$  to  $A_{c2}^{(2)}$ , the radius of the spot will grow. However, at certain radius corresponding to the value of  $A = A_{c2}^{(2)}$  the spot becomes unstable with respect to the radially-nonsymmetric distortions of its walls [11,12,23,30]. Qualitatively, this means that a “burning spot” tends to ignite the neighboring regions, but since its radius is bounded from above, the only way it can grow in size is by elongation. Precisely this phenomenon was observed in the simulations. For  $A < A_{c3}^{(2)} \simeq -0.46$  the spot elongates and transforms into a stripe. If  $A > A_{c3}^{(2)}$ , the tips of the growing stripe

become further unstable, leading to the tip splitting and the formation of a labyrinthine pattern. This effect is seen in the simulation of Fig. 5, where  $A = -0.4$ , which is not much greater than  $A_{c3}^{(2)}$ . There an almost radially-symmetric spot at  $t = 0$  elongated and transformed into a dumbbell at  $t = 63$  and then further destabilized into a more complex shape at  $t = 98$ . The process of tip splitting resulted in a more and more complicated pattern at  $t = 162$  and  $t = 292$ , until the resulting labyrinthine pattern reached the system boundaries and stopped growing at  $t = 985$ . Similar structures were also observed in the simulations in Refs. [31,32] and in chemical reactions [6,8,17]. The labyrinthine pattern that formed in the end is a collection of stripe-like domains which are all connected. Notice that in this simulation  $\alpha = 0.2$ . However, the smallness of the value of  $\alpha$  does not affect the simulation results as long as  $\alpha \gg \epsilon$ . On the other hand, this choice of  $\alpha$  significantly accelerates the simulations.

In the next simulation we took  $A = -0.25$ , which is further away from  $A_{c2}^{(2)}$  and closer to  $A_c$ . The initial conditions were taken in the form of the homogeneous state plus a piece of a curved stripe. One can see (Fig. 6) that initially ( $t = 22$ ) the tips of the pattern grow faster and start splitting ( $t = 87$ ). One can also see that the stripe itself start to wriggle, and fingers spring out of the regions with the highest curvature ( $t = 118$ ). However, in contrast to the previous case, some of the portions of the growing labyrinthine pattern detach themselves from the body of the pattern. As the time passes, more and more portions become detached. In the end the labyrinthine pattern that fills the whole system at  $t = 322$  consists of 5 disconnected pieces. Notice the great similarity between this pattern and the labyrinthine pattern formed as a result of Turing instability in Fig. 4. Also notice that the disconnected pattern is more likely to form even for  $A$  not very different from  $A_{c2}^{(2)}$ , if  $\alpha$  is smaller. This is because at small  $\alpha$  the dynamics of the pattern becomes oscillatory and the labyrinthine pattern may form as a result of self-replication of spots, which will be discussed below.

The same picture can be observed, if the initial conditions are taken in the form of a twisted stripe running across the system, if  $A$  is big enough. In general, for  $A$  considerably greater than  $A_b$  any localized initial condition will lead to the formation of the disconnected labyrinthine pattern. However, if these boundary conditions are used with the values of  $A$  closer to  $A_b$ , a wriggled stripe pattern will form in the system. This process is related with the fact that a stripe may become unstable with respect to wriggling of the stripe as a whole while being stable with respect to fingering when  $A_{c1}^{(1)} < A < A_{c1}^{(1)}$  [11,12,23,30]. For  $\epsilon = 0.05$  the value of  $A_{c1}^{(1)}$  obtained from the simulations is  $A_{c1}^{(1)} \simeq -0.32$ . The evolution of the stripe at  $A = -0.45$  is shown in Fig. 7. One can see that the stripe gets more and more wriggled without fingering for a long time. Only when the curvature of some portion of the stripe becomes sufficiently

high, a finger springs out ( $t = 1418$ ). Notice that fingering also occurs at the points where the stripe is attached to the boundary. At these points the curvature of the stripe is high as well.

Up to now we considered the pattern formation in the stable KN system in which the inhibitor is fast. According to our simulations, the time scale of the inhibitor variation does not affect all the results above when  $\alpha \ll 1$  but  $\alpha \gg \epsilon$ . In  $K\Omega N$  systems, in which the inhibitor is slow enough, pattern formation scenarios will be qualitatively different. Figure 8 shows the evolution of the system at  $A = -0.4$ , but  $\alpha = 0.015$  with the initial condition in the form of an almost radially-symmetric spot. In contrast to the simulation of Fig. 5 which was performed for the same value of  $A$  and with the same initial conditions, instead of transforming into a dumbbell the spot splits into two in the course of its evolution ( $t = 3.3$ ). The spots that form split in turn into four ( $t = 5.2$ ). This process of self-replication of spots continues until the whole system is filled with the multidomain pattern (not shown in the figure), which may stabilize or transform into a synchronously pulsating (breathing) pattern. Notice that self-replication of spots was observed in the chemical experiments [16,17] and in the simulations [31]. A similar phenomenon also seems to occur in the chaotic cellular flames [22].

Figure 9 shows the value of  $\eta$  in the center of the system in which the synchronously pulsating multidomain pattern formed as a result of spot self-replication. One can see that the multidomain pattern forms at relatively short times ( $t \lesssim 5$  for the system  $10 \times 10$ ), and after that the oscillation of the pattern as a whole starts. Some restructuring of the pattern occurs later on, what results in the changes of the oscillations amplitude and the pattern's geometry. At times  $t \gtrsim 120$  the pattern's oscillations had synchronized and no changes in the oscillations amplitude nor in the pattern's geometry were observed in the longer runs.

The mechanism of self-replication can be seen from Fig. 10, where a single self-replication event is shown in detail. One can see that self-replication is determined by the two processes: radially-symmetric pulsations of the spot's radius and aperiodic growth of the non-symmetric distortion. At the beginning the spot expands as a whole ( $t = 0.6$ ), but at the same time the non-symmetric distortion builds up ( $t = 1.4$ ). Then the spot starts to shrink in the course of the radially-symmetric pulsations, so the connection between its right and left portions gets torn at  $t = 2.1$ . At  $t = 2.6$  there are two spots looking just like the one at  $t = 0$  in the system. Notice that for smaller values of  $A$  a single self-replication act may take more than one pulsation period.

When the value of  $\alpha$  is smaller, the process of self-replication of domains may become stochastic, producing a kind of turbulence (Fig. 11). In the simulation of Fig. 11 ( $\alpha = 0.01$ ,  $A = -0.4$ ) the initial condition in the form of a small domain initially grows in size, but at  $t = 1.2$  local breakdown occurs in its center, so that

the domain transforms into an annulus. The annulus then splits in turn into several smaller domains ( $t = 5.3$ ) which engage into incessant stochastic motion. Each domain is self-replicating, but some of the domains formed as a result of this process die as a result of the collisions with the other domains, what causes the stochastization. Another source of stochastization is the local breakdown which occurs, if the domain size becomes too big. The number of domains in the system changes randomly with time. Each domain is also moving as a whole. The interaction between different domains (and the boundaries) is repulsive, so the domain fusion is typically avoided. The turbulent pattern is persistent and does not synchronize even after long times (Fig. 12). It is observed only at sufficiently large values of  $A$ . When  $A$  is relatively small, the turbulent pattern usually collapses into the homogeneous state after relatively short times. This kind of turbulence was observed in the chemical [16,17] and combustion [22] experiments. Notice that the turbulence that is observed in our simulations is different from the spiral turbulence observed by Hagberg and Meron [31]. In our simulations we never saw the nucleation of the spiral vortex pairs.

When the value of  $\alpha$  is even smaller, a localized initial perturbation transforms into an autowave. In the simulation of Fig. 13(a), in which  $\alpha = 0.007$ ,  $A = -0.3$ , the domain expands, and at  $t = 1.1$  it transforms into an annulus which now remains stable and continues to expand. This results in an autowave passing through the system and annihilating when it reaches the boundaries. In this case there is no repulsion between the autowaves. At these and smaller  $\alpha$  only autowaves form in the system, regardless of the value of  $A$ . If a random initial condition is taken, spiral turbulence typical of the excitable autowave media ( $\Omega N$  systems) will form at  $\alpha \ll \epsilon$  [Fig. 13(b)]. Here the turbulent pattern consists of a random arrangement of spiral vortices whose positions are fixed in space. The spiral waves always annihilate upon collision in this case. This is a well-known phenomenon in the  $\Omega N$  systems (excitable media), for which  $L = 0$  [3,5,8].

Before concluding this Section, let us mention two other simulations. In the first [Fig. 13(c)], for which  $\alpha = 0.02$  and  $A = -0.3$ , a localized initial perturbation results in a few replication-like acts, but after that the pattern stabilizes into a static disconnected labyrinthine pattern. In the second the value of  $\epsilon = 0.2$  was taken to be not very small (the other parameters are  $\alpha = 1.$ , and  $A = -0.1$ ), so that the system is away from the asymptotic regime  $\epsilon \rightarrow 0$  [Fig. 13(d)]. One can see from Fig. 13(d) that the localized initial perturbation transforms into a disconnected labyrinthine pattern in this case as well, so, qualitatively, the effects observed in this Section are realized when the value of  $\epsilon$  is not very small.

The patterns which were described above are the only kinds of patterns that were observed in the system under consideration. No other types of patterns were observed in the simulations, no matter what initial conditions or the parameters  $\alpha$ ,  $\epsilon$ , and  $A$  were used (of course, there are "cold" patterns, but in view of Eq. (9) they are equiv-

alent to the “hot” patterns studied above). Thus, these patterns constitute the totality of the pattern types of the considered system.

#### IV. DOMAINS OF EXISTENCE OF DIFFERENT TYPES OF PATTERNS AND SCENARIOS OF PATTERN FORMATION

In this Section we will analyze the pattern formation scenarios observed in the previous Section, give quantitative explanation for the parameter regions in which different patterns form, and explain the transformations of one type of pattern to the other on the basis of the general asymptotic theory of instabilities for patterns with sharp interfaces developed by us in Ref. [23], and on the basis of the interfacial dynamics approaches developed in Refs. [30,32,33].

Our simulations of the spontaneous formation of Turing patterns confirm the conclusion of the general qualitative theory that at the threshold of Turing instability large-amplitude patterns should form abruptly in the system [10,12]. According to Eq. (12), for small  $\epsilon$  Turing instability occurs at  $A \simeq A_0 = -1/3\sqrt{3} \simeq -0.19$ , with respect to the fluctuations with the wave vector  $k_c \simeq \epsilon^{-1/2}$ . One can see from Fig. 3 that at early stages ( $t = 16$ ) there are many domains of small size, so one could naturally assume that at early stages the domain sizes are determined by the wavelength of the critical fluctuations, which is of order  $\epsilon^{1/2}$ . However, as can be seen from Fig. 3, at late stages the average size of the domains becomes greater and in the end all domains have roughly the same size. This is not surprising since the domains of small size are unstable because of the effect of the activator repumping [10,12]. The thing is that because of its long-range character, it is difficult for the inhibitor to react on such variations of the activator that lead to the expansion of some of the domains and the simultaneous shrinkage of their neighbors. This can be seen from the estimate of the terms in the dispersion relation for the fluctuations around the Turing pattern. For simplicity let us consider a hexagonal arrangement of circular domains of radius  $\mathcal{R}_s$  with the period  $\mathcal{L}_p$ . Then the fluctuation which leads to the activator repumping has the wave vector  $k = \pi/\mathcal{L}_p \gg 1$  for  $\mathcal{L}_p \ll 1$ . The term in the dispersion relation that causes the instability is  $\lambda_0 \simeq -\epsilon^2/\mathcal{R}_s^2$  [11,12,23], whereas the inhibitor reaction term, which has the stabilizing effect, is of order  $\epsilon\mathcal{L}_p$  [10,12], and the values of  $\mathcal{L}_p$  and  $\mathcal{R}_s$  are of the same order. Therefore, when  $\mathcal{R}_s$  is smaller than  $\mathcal{R}_b \sim \epsilon^{1/3}$ , this fluctuation will grow and lead to the expansion of every second domain and collapse of the rest, what will result in the increase of the pattern’s period and the radius of the domains. In other words, the domains will grow by eating their neighbors until their size and the distance between them becomes of order  $\epsilon^{1/3}$ .

On the other hand, the domain radius cannot be

greater than  $\mathcal{R}_{c2} \sim \epsilon^{1/3}$  since at greater radii the domain becomes unstable with respect to the non-symmetric deformations and either splits or elongates. The important thing, however, is that both  $\mathcal{R}_b$  and  $\mathcal{R}_{c2}$  are much greater than  $2\pi/k_c \sim \epsilon^{1/2}$  for small  $\epsilon$ , so the process of formation of Turing pattern must always consist of two stages: initial domain forming and ripening.

Notice that in the presence of small localized inhomogeneities the process of formation of Turing pattern may be qualitatively different [11,12]. A small localized domain may nucleate at the inhomogeneity, but then as a result of the transverse instability of its walls, which occurs when the domain radius becomes of order  $\epsilon^{1/3}$  [23], it will transform into a disconnected labyrinthine pattern, if  $\epsilon$  is not very small, or start to split and replicate itself until the system is filled with the domains of size of order  $\epsilon^{1/3}$ , if  $\epsilon$  is very small [33]. These effects will occur when  $\alpha \gg \epsilon$ .

According to Eqs. (11) and (12), Turing instability is the first if  $\alpha > 2\epsilon$  for small  $\epsilon$ . However, as we see from the simulations, even for smaller values of  $\alpha$ , that is, when the homogeneous state of the system is unstable with respect to both Turing and oscillatory instability, static Turing patterns may persist up to smaller values of  $\alpha$ . For  $\epsilon = 0.05$  this happens down to  $\alpha \simeq 0.02$ . For these values of  $\alpha$  one can see the competition between the Turing patterns and the uniform self-oscillations. For  $\alpha < 0.02$  the uniform self-oscillations win, and Turing patterns do not form. For  $\alpha > 0.02$  the situation is reverse. We did not observe the coexistence of Turing patterns and uniform self-oscillations. It is interesting to note, however, that the well-formed Turing pattern may be stable for even smaller values of  $\alpha$ . Also, if there are small local inhomogeneities in the system with  $\alpha \sim \epsilon$ , the system will nucleate localized domains before reaching the instability, as in the case of  $\alpha \gg \epsilon$ , but then the domains will self-replicate and a multidomain pattern will form in the system. If the value of  $\alpha$  is smaller, the inhomogeneities will cause nucleation of guiding centers [11,12].

Let us now turn to the patterns that are excited in the system with the stable homogeneous state. Our first observation is that, as was expected [11,12] and in agreement with the statements of Fife [34], any localized initial perturbation at first relatively quickly transforms into a state in the form of the domain with sharp walls, which is the closest to the initial perturbation in shape, and then this domain starts to evolve considerably slower according to the equations of the interface dynamics. The characteristic time scale for the domain to form is that of the activator, that is  $\alpha$ , and the characteristic time scale of the interface motion is  $\alpha/\epsilon$  [33], so one can see that as long as  $\epsilon \ll 1$  the latter time is much longer than the former. In this sense one could think that at first the initial perturbation evolves into a closest in shape stationary state, which then grows into a more complicated stable pattern as a result of the instability of that state. In this process the early stages of the formation of a complex

pattern is determined by the type of the critical fluctuation with respect to which that stationary state loses its stability. Therefore, it is important to know the form of possible stationary states and when they become unstable.

The simplest patterns in the considered system are static spots and stripes [11,12,30]. They are indeed observed when  $A$  is sufficiently close to  $A_b$ , when a spot-like or stripe-like initial perturbations are used, respectively. We performed numerical simulations of the one-dimensional and radially-symmetric versions of Eqs. (7) and (8) and found the dependences of the stripe's width  $\mathcal{L}_s$  and the spot's radius  $\mathcal{R}_s$  versus  $A$  at  $\epsilon = 0.05$  (Fig. 14). From these simulations one can see that the solution in the form of a single static stripe exists at  $A_b^{(1)} < A < A_c$ , where  $A_b^{(1)} = -0.74$ , whereas the solution in the form of a single static spot exists when  $A_b^{(2)} < A < A_d^{(2)}$ , where  $A_b^{(2)} = -0.72$  and  $A_d^{(2)} = -0.24 < A_c$ . When  $A_d^{(2)} < A < A_c$ , the local breakdown occurs in the spot's center, so the spot transforms into an annulus. The thing is that for  $\epsilon \ll 1$  the distributions of the activator and the inhibitor outside the walls of the spot are related via the equation of local coupling [10–12,23]

$$q(\theta, \eta) = 0. \quad (13)$$

In other words,  $\theta$  and  $\eta$  lie on one of the stable branches of the nullcline of Eq. (7):  $\theta < \theta_0$  in the cold region and  $\theta > \theta'_0$  in the hot region (Fig. 1). As the radius of the hot spot grows the value of  $\eta$  in its center gets smaller, so at some value of  $A = A_d^{(2)} < A_c$  it reaches  $\eta'_0$ , the point at which the dependence  $\theta(\eta)$  determined by Eq. (13) becomes singular, so a sudden down-jump from one branch of the nullcline to the other occurs, resulting in the formation of a new interface in the spot's center and the transformation of the spot into an annulus. Notice that the process of local breakdown in the center of a spot and the formation of an annulus in N systems was studied in detail in Refs. [11,12]. Also notice that the same mechanism is responsible for the local breakdown in the center of a one-dimensional stripe [11,12]. However, it does not occur in the particular system we study.

In higher dimensions spots and stripes undergo instabilities leading to the growth of certain deformations of their walls. Recently we developed a general asymptotic theory of the instabilities of domain patterns in arbitrary N systems [23]. We have shown that the instabilities are determined by the motion and the interaction of the pattern's walls (interfaces). For sufficiently small  $\epsilon$  one could use the formulas obtained in Ref. [23] and the dependences  $\mathcal{L}_s(A)$  and  $\mathcal{R}_s(A)$  to determine the critical values of  $A$  at which one or another instability of the spots and stripes occur. The parameters that enter those formulas for the considered system are

$$B = 4, \quad Z = \frac{2\sqrt{2}}{3}, \quad C = \frac{3}{2}. \quad (14)$$

However, for  $\epsilon = 0.05$  the agreement between the results of the simulations and the predictions of Ref. [23] is rather crude (about 50%). This is due to the fact that in the derivations of the critical values of the domain sizes, which are typically of order  $\epsilon^{1/3}$ , we used them as small parameters. However, because of the slow  $\epsilon$ -dependence (1/3 power) this is not a very good assumption for  $\epsilon \simeq 0.05$ .

Nevertheless, there is a way to calculate the critical values of  $\mathcal{L}_s$  and  $\mathcal{R}_s$  which agree with the results of the simulations with the accuracy better than 5%. To do this, we can use the dispersion relations obtained in Ref. [23] in the zeroth order of the perturbation theory in the potential  $V$ , but not expanding in  $\mathcal{R}_s$ , or  $\mathcal{L}_s$ , respectively, and keeping the value of  $C$  evaluated at  $A = A_b$ . The latter is because the critical fluctuations are localized in the walls of the pattern and this is the way to take into account some of the potential  $V$ . Having done this, for the stripes we have the following dispersion relation

$$i\alpha\omega + \epsilon^2 k^2 + \lambda_0 = -\frac{\epsilon B Z^{-1}}{2\sqrt{C + k^2 + i\omega}} \left( 1 \pm \exp(-\mathcal{L}_s \sqrt{C + k^2 + i\omega}) \right), \quad (15)$$

where the constants  $B$ ,  $C$ , and  $Z$  are defined in Eq. (14),  $k$  is the wave vector along the stripe,  $\omega$  is the frequency, the “+” sign corresponds to the symmetric, the “-” sign corresponds to the antisymmetric deformations of the stripe, and

$$\lambda_0 = -\frac{\epsilon B (1 - e^{-\mathcal{L}_s \sqrt{C}})}{2Z\sqrt{C}}. \quad (16)$$

Similarly, for the spots we will have the following dispersion relation

$$i\alpha\omega + \frac{\epsilon^2 m^2}{\mathcal{R}_s^2} + \lambda_0 = -\epsilon B Z^{-1} I_m(\mathcal{R}_s \sqrt{C + i\omega}) K_m(\mathcal{R}_s \sqrt{C + i\omega}), \quad (17)$$

where  $I_m$  and  $K_m$  are the modified Bessel functions,  $m$  is an integer corresponding to the  $m$ -th surface mode, and  $\lambda_0$  in this case is

$$\lambda_0 = -\frac{\epsilon^2}{\mathcal{R}_s^2} - \epsilon B Z^{-1} I_m(\mathcal{R}_s \sqrt{C}) K_m(\mathcal{R}_s \sqrt{C}). \quad (18)$$

The instabilities occur when  $Im \omega < 0$ . These transcendental equations can be solved for  $\mathcal{L}_s$  and  $\mathcal{R}_s$ , respectively, when  $Im \omega = 0$ , for given  $k$  or  $m$ . Then, using the dependences shown in Fig. 14, one can find the critical values of  $A$  at which different types of the instabilities occur.

Let us consider the case of the fast inhibitor  $\alpha \gg \epsilon$ . Then, according to Eq. (17), at  $A = A_{c2}^{(2)} = -0.56$  the spot will become unstable with respect to the  $m = 2$  mode, which corresponds to a dumbbell-shaped deformation. Also, from Eq. (17) follows that the spot destabilizes with respect to the  $m = 0$  mode if  $A < A_b^{(2)} =$



-0.72. This is in perfect agreement with the results of the simulations.

Similarly, according to Eq. (15), the stripe becomes unstable with respect to antisymmetric fluctuations (wriggling) at  $A > A_{c2}^{(1)} = -0.61$ , and with respect to symmetric fluctuations (corrugation) at  $A > A_{c1}^{(1)} = -0.32$ . The minimum width of the stripe is determined by the overlap of the fluctuations of the activator, so it is not taken into account in Eq. (15) [11,12,23]. If we do take it into account, we will obtain that the stripe is unstable at  $A < A_b^{(1)} = -0.74$ . So, here the agreement between the predictions of the theory and the simulations is excellent as well.

The type of the complex pattern that forms in the late stages of the destabilization of the simple patterns is determined by the dynamics of its interface. For description of pattern dynamics in higher-dimensional N systems Ohta, Mimura and Kobayashi developed an approach which allowed them to reduce the equations similar to Eqs. (1) and (2) to the problem of the interface dynamics in the case of slow inhibitor in the limit  $\epsilon \rightarrow 0$  and analyzed the early stages of the transverse instability development [30]. Goldstein, Muraki and Petrich derived an equation of the interface dynamics for a simple system of FitzHugh-Nagumo type in the limit of fast inhibitor and weak activator-inhibitor coupling and showed that the destabilization of simple patterns lead to the formation of the connected labyrinthine patterns [32]. Muratov derived the general equation of the interface dynamics for N systems described by Eqs. (1) and (2) and showed that in the limit  $\epsilon \rightarrow 0$  and  $\alpha \gg \epsilon$  only multidomain patterns must form as a result of the instability and self-replication of simple patterns [33]. However, because of the slow dependences of certain parameters on  $\epsilon$ , multidomain patterns should in fact form only at  $\epsilon \lesssim 0.01$  in the considered system [33]. Yet the interfacial approach remains a good approximation for the dynamics of the pattern for  $\epsilon = 0.05$ . In this sense the region  $0.01 \lesssim \epsilon \ll 1$  can be considered a ‘‘crossover’’ region between the labyrinthine and the multidomain patterns. This is the reason why we see both connected and disconnected labyrinthine patterns in our simulations. When  $A$  is not far from  $A_{c2}^{(2)}$  the transverse instability is not very strong, so connected labyrinthine patterns form (Fig. 5). Here the stripe shape is more favorable than the spot shape. As was noticed in the previous Section, when  $A$  is close to  $A_{c2}^{(2)}$  (in the simulations we used  $A = -0.50$ ), a spot destabilizes into a single stripe which does not branch. This may be qualitatively explained by the following argument. In order for branching to occur, a spot has to be unstable with respect to the  $m = 3$  mode. According to Eq. (17), this should happen at  $A > A_{c3}^{(2)} = -0.45$ . For  $A_{c2}^{(2)} < A < A_{c3}^{(2)}$  the stripe is in turn unstable with respect to wriggling, so as a result of the instability of a spot for those values of  $A$  the wriggled stripe (Fig. 7) will eventually form in the system. This is precisely what we

see in our simulations.

When the value of  $A$  gets larger, the transverse instability gets stronger and the spot shape becomes more favorable. There we see domain splitting predicted in Ref. [33] and, therefore, the *disconnected* labyrinthine pattern, which is the counterpart of the multidomain pattern in this case. We emphasize that this will happen only when  $\epsilon$  is relatively large; according to our simulations, indeed, for  $\epsilon \leq 0.01$  only multidomain patterns form in the system.

Another important thing about the complex domain patterns is that the multidomain patterns may coexist with the labyrinthine patterns. As was shown by Muratov, for the same values of the parameters  $\epsilon$ ,  $\alpha$  and  $A$  one could excite both multidomain and labyrinthine patterns by choosing appropriate initial conditions [33]. For example, one could take the pattern that formed in the end of the simulation of Fig. 3 and use it as an initial conditions for the run with the value of  $A$  corresponding to the stable homogeneous state. Then in the course of the system’s evolution the domains will shrink and some of them will disappear, but in the end the system will be filled with the multidomain pattern similar to the one in Fig. 3 ( $t = 955$ ), rather than with the labyrinthine pattern.

Recently, Hagberg and Meron studied numerically the formation of labyrinthine patterns in a bistable N system and explained this effect on the basis of the non-trivial properties of solitary fronts that form only in bistable systems [35]. However, according to the experimental observations [17] and our numerical simulations, labyrinthine patterns may form both in monostable and bistable systems. In order to make the system of Eqs. (7) and (8) bistable one needs to add a coefficient  $\gamma$  in front of  $\theta$  on the right-hand side of Eq. (8). Then for  $\gamma = 1$  the system will be monostable, whereas for smaller  $\gamma$ , for example  $\gamma = 0.5$ , the system is bistable. We did not see any qualitative difference between the patterns in these two cases. In the monostable systems the solitary fronts do not exist at all, so the domains always have finite width at least in one direction. The properties of such patterns are different from those of the solitary fronts, and are essentially determined by the non-local interaction of different portions of the pattern’s interfaces [11,12,23,33]. Besides, in the bistable systems with  $\gamma \gg \epsilon$  and  $\epsilon \ll 1$  the solitary fronts are always unstable with respect to the transverse instability. Indeed, according to Eq. (15) with  $B = 4\gamma$ ,  $C = 1 + \frac{1}{2}\gamma$ , and  $\mathcal{L}_s = \infty$ , the front is unstable with respect to the transverse perturbations with the wave vector  $k \sim \epsilon^{-1/3}$ . So, in general one cannot use the properties of the solitary fronts to explain the formation of complex domain patterns in N systems. Notice that according to the similar argument, any pattern whose characteristic size is much greater than  $\epsilon^{1/3}$  is unstable with respect to transverse perturbations both in the monostable and bistable systems.

Let us now consider the case of slow inhibitor  $\alpha \lesssim \epsilon$ . Since the prevailing shape in the simulations in this case

is a spot, we will look for the instabilities of the circular domain. We solved Eq. (17) in the case  $\alpha \lesssim \epsilon$  for  $m = 0, 1$  and 2. We found qualitative agreement with the results of the general asymptotic theory for instabilities of domain patterns [23].

For  $m = 0$  the instability occurs at  $Re \omega \neq 0$ . This instability leads to the transformation of the static spot into a radially-symmetric pulsating (breathing) spot. Such pulsating spots were observed in the numerical simulations and the experiments [10–12,36,37]. The instability occurs when the radius of a spot  $\mathcal{R}_\omega^{min} < \mathcal{R}_s < \mathcal{R}_\omega^{max}$ , where  $\mathcal{R}_\omega^{min}$  and  $\mathcal{R}_\omega^{max}$  are the functions of  $\alpha$ . For  $\epsilon = 0.05$  and  $\alpha \gtrsim 0.02$  the spot is stable in the whole region of its existence. For  $\alpha < 0.009$  the spot is unstable for all  $\mathcal{R}_s$ .

The  $m = 1$  instability leads to the transformation of a static spot into traveling. According to Eq. (17), a spot becomes unstable with respect to the  $m = 1$  mode when  $\mathcal{R}_s > \mathcal{R}_T$ , where  $\mathcal{R}_T$  is a function of  $\alpha$  and  $A$ . Notice that the general criterion of such transformations was obtained by Osipov in Ref. [38]. For the same values of  $A$  the  $m = 1$  instability always happens at smaller values of  $\alpha$  than the  $m = 0$  instability. The instabilities for  $m \geq 2$  with  $Re \omega \neq 0$  occur at even smaller values of  $\alpha$ , when the spot is already unstable with respect to  $m = 0$  and  $m = 1$  modes.

The results of the analysis of the instabilities of simple shapes (spots and stripes) and the results of the numerical simulations can be presented on the diagram (Fig. 15). This diagram shows the domains of existence of different types of patterns in the  $\alpha - A$  plane for  $\epsilon = 0.05$  when the homogeneous state of the system is stable. All the simulations points, which are marked by Roman letters in Fig. 15, were obtained by using localized initial conditions. The vertical lines in Fig. 15 correspond to the values of  $A$  at which different instabilities of the domain shapes occur, calculated from Eqs. (15) and (17). One can see that these lines separate the regions in which the corresponding types of static patterns are observed in the simulations. The letter “s” corresponds to the simulations in which the aperiodic relaxation was observed. The upper dashed line separates the region in which any initial condition relaxes aperiodically to one of the static patterns from the region in which the relaxation becomes oscillatory. As was expected [11,12], the transition from the aperiodic to the oscillatory relaxation occurs at  $\alpha \sim \epsilon$ . Above the upper dashed line the form of the patterns is essentially independent of  $\alpha$ ; depending on the value of  $A$  and the initial condition one can see spots, stripes, wiggled stripes, multidomain patterns and labyrinthine patterns (Figs. 3, 5, 6, 7). Of course, for  $\epsilon = 0.05$  one should use special initial conditions (not localized) to excite the multidomain patterns.

Below the upper dashed line but above the upper solid line the relaxation of the initial excitation of the system results in the formation of a stable static pattern, although a few pulsations and spot splittings associated with them may occur at the beginning [Fig. 13(c)], so

the resulting pattern is disconnected for all values of  $A > A_{c2}^{(2)}$ . The simulations of this type are marked “ps” in Fig. 15. Notice that in this parameter region self-replication of spots does not occur, but the fact that the inhibitor is slow makes the domain splitting easier, since the inhibitor lags behind the motion of the interface driven by the transverse instability of the spot [33].

The upper solid line represents the solution of Eq. (17) for  $m = 0$  and shows the instability line for a spot with respect to pulsations (breathing). The simulations show that below this line different dynamic patterns form. When  $A$  is big enough and  $\alpha$  is just slightly below the upper solid line, spot replication leading to the formation of static or synchronously pulsating pattern is observed (Fig. 8). These simulations are marked by “p” in Fig. 15. As was already mentioned above, for  $\epsilon = 0.05$  self-replication does not occur when the inhibitor is fast. Nevertheless, self-replication does occur in the case of the slow inhibitor ( $\alpha \lesssim \epsilon$ ). In this case the transverse instability, which is the primary cause of the domain splitting and self-replication [33], is assisted by the instability which leads to the radially-symmetric pulsations. This is the reason why spot replication does not occur above the upper solid line, which is the pulsation instability threshold for a spot.

As can be seen from Fig. 15, the dominant type of dynamic patterns for  $\alpha \sim \epsilon$  is the turbulence (Fig. 11, the points marked “t” in Fig. 15). When the two spots come at distances less or of order 1 to each other, the inhibitor may not be able to suppress the growth of one spot due to the shrinkage of the other (the activator repumping effect) what may result in the disappearance of one of the spots. However, the surviving spot may self-replicate in turn and create another spot. Also, if a spot does not have other spots around, it may transform into an annulus as a result of the local breakdown in the spot’s center, and the annulus may then break up into a number of spots as a result of the transverse instability. It is these three processes uncorrelated in space that make the turbulence possible in the K $\Omega$ N systems.

The turbulence is observed at relatively large values of  $A$ . This is not surprising. Since the turbulence is caused by the self-replication process, it may occur only when the spot is able to replicate, that is, when  $A > A_{c2}^{(2)}$ . For smaller values of  $A$  the spots do not self-replicate, instead they collapse after a few periods of pulsations (simulations marked “c” in Fig. 15). The meaning of the separation between the region where the turbulence and the synchronously pulsating patterns are realized is less obvious. Qualitatively, the disappearance of some of the domains in the course of the pattern’s dynamics and the local breakdown, the processes that cause the stochasticization, occur easier when the inhibitor is slower, that is, when  $\alpha$  is smaller. Of course, in order to make a quantitative explanation of this separation, one has to solve a highly nonlinear free-boundary problem in two dimensions.

All the dynamic patterns mentioned above are observed above the lower solid line, which is the stability margin for a spot for  $m = 1$  obtained from Eq. (17). Below this line a static spot destabilizes and transforms to traveling. In this region only autowaves (the simulations marked “a”) form from a localized initial perturbation [Fig. 13(a)]. The autowave patterns that form below the lower solid line are essentially the same for all values of  $\alpha$  (aside from the time and length scales of the pattern) and in fact do not differ from the autowaves forming in  $\Omega N$ -systems with  $\epsilon \gtrsim 1$ . This is because at  $\alpha \ll \epsilon$  the diffusive precursor is not able to form in front of the traveling pattern front [11,12]. Observe that according to Fig. 15, no complex static or dynamic patterns (except autowaves) form in the system at any  $A$  if  $\alpha \lesssim \epsilon^2$ . This fact is in total agreement with the general qualitative theory [10–12] and with the conclusions of the general asymptotic theory of instabilities [23,38].

Hagberg and Meron explained self-replication of spots and formation of turbulence as the consequences of the parity-breaking bifurcations [nonequilibrium Ising-Bloch (NIB) front transitions] of the planar fronts in bistable  $N$  systems with the weak activator-inhibitor coupling [35]. Although their approach is useful for the qualitative or heuristic explanation of the formation of the dynamic patterns discussed above, it is highly inadequate for making quantitative predictions in general. Indeed, the process of self-replication observed in our simulation cannot be viewed as a consequence of local NIB transitions (reversal of the propagation direction of the portions of the spot’s interface), since, according to our numerical simulations, the *whole* spot’s interface reverses its propagation velocity in the course of self-replication (Fig. 10). Furthermore, as can be seen from Fig. 15, the region of the system’s parameters in which spot self-replication is realized is determined by the instabilities of the static spot, and not of the planar front, or the planar stripe, which is the counterpart of the planar front for the monostable systems. One can show that according to Eq. (15), both the instability of the stripe with respect to pulsations [the “+” sign in Eq. (15)] and the instability leading to the transformation of the static stripe into traveling [the “–” sign in Eq. (15)] lie considerably lower than both solid lines in Fig. 15, which correspond to the respective instabilities of the spot. Hagberg and Meron predict domain splitting and formation of disconnected labyrinthine patterns only close to the NIB transitions (where  $\alpha \sim \epsilon$ ) [35], and yet domain splitting and the formation of disconnected labyrinthine pattern occurs solely due to the transverse instability far from the presumed NIB transitions (Fig. 6). Also, as was already mentioned, the turbulence that was observed in our simulations is different from the spiral turbulence observed by Hagberg and Meron in the bistable system with relatively weak activator-inhibitor coupling [31,35]. One could think of the turbulence observed by Hagberg and Meron as intermediate between the spiral turbulence observed in the excitable autowave media ( $\Omega N$  systems) and the turbu-

lence observed by us in a  $K\Omega N$  system. In our simulations the nucleation of spiral vortex pairs is not allowed by the local breakdown. The turbulence is produced by the constant self-replication of spots with the stochasticization caused by the disappearance (annihilation) of some of the domains because of their strong interaction with the neighbors, and the spontaneous creation of new interfaces (transformation of a spot into an annulus) due to the local breakdown, which occurs, if the size of the domain becomes big enough (Fig. 11). All this suggests that in the general  $N$  systems with  $\epsilon \ll 1$  strong non-local interaction between the different portions of the domain interfaces and between different domains, high curvature of the domain interfaces, the time lag between the motion of the interface and the reaction of the inhibitor, and the process of local breakdown are crucial and in fact determine the type of the pattern that will form in the system from a localized stimulus for the given values of the system’s parameters.

Before concluding this Section, let us discuss how the changes in the values of  $\epsilon$  should affect the bifurcation sequences and the pattern formation scenarios in the considered systems. As was already mentioned, the value  $\epsilon = 0.05$  corresponds to a “crossover” between the asymptotically small values of  $\epsilon$ , and the relatively large  $\epsilon \sim 1$ . The value of  $\epsilon = 0.05$  is reasonably small to admit strong separation of the length scales of the activator and the inhibitor, yet it is not very small in the asymptotic sense, for which in the considered model we should have  $\epsilon \lesssim 0.01$ . It is clear that if the value of  $\epsilon$  is increased, the transverse instabilities will become weaker, so the vertical lines corresponding to the instabilities of a spot in Fig. 15 will move to the greater values of  $A$ . For these values of  $\epsilon$  and  $\alpha \gg \epsilon$  the stripe shape will become dominant over the spot shape, so the typical complex pattern forming in the system will be the labyrinthine pattern which consists of long wriggled stripes, which may still be disconnected [Fig. 13(d)]. This will also be true for the Turing patterns forming as a result of the instability of the homogeneous state. If the value of  $\alpha$  gets smaller, the turbulent patterns will form. Our simulations show that in this situation the pattern’s oscillations are less likely to synchronize than in the case of smaller  $\epsilon$  because of the stronger stochasticization due to the local breakdown, so it would be easier for the turbulent patterns to form. If  $\epsilon$  is even greater, the patterns can no longer be viewed as having sharp interfaces, so the entire phenomenology of pattern formation will change.

On the other hand, if the value of  $\epsilon$  is decreased, the transverse instability will become stronger, and the dominant shape will become the spot shape. In this case all vertical lines which correspond to the instabilities of a spot in Fig. 15 will move toward  $A = A_b$ . In the case  $\alpha \gg \epsilon$  only disconnected labyrinthine patterns or multidomain patterns will form as a result of the transverse instability [33]. The characteristic size of such patterns will be  $\epsilon^{1/3}$  [23,33], so at very small  $\epsilon$  any spot will interact with many other spots. Because of this interaction,

for  $\alpha \lesssim \epsilon$  the pulsating patterns will tend to synchronize more, so the synchronously pulsating multidomain patterns should exist in a wider range of the system's parameters. Also, as follows from the general asymptotic theory of instabilities [23], for extremely small  $\epsilon$  ( $\epsilon \lesssim 10^{-6}$ ) the instability of a spot with respect to the fluctuations leading to the formation of a traveling spot will always occur at larger values of  $\alpha$  than the pulsating instability, so it is natural to conclude that complex dynamic patterns, such as pulsating multidomain patterns and turbulent patterns, cannot be excited by a localized stimulus at such small values of  $\epsilon$ .

## V. CONCLUSION

In this paper we performed a complete numerical study of different types of domain patterns in a two-dimensional N system and investigated all major scenarios of their formation. We confirmed the conclusions of Kerner and Osipov [10–12] that the type of the domain patterns forming in the N systems is determined mainly by the two basic parameters of the system:  $\alpha = \tau_\theta/\tau_\eta$  and  $\epsilon = l/L = \sqrt{D_\theta\tau_\theta/D_\eta\tau_\eta}$ . These parameters are the ratios of the characteristic time and length scales of the variation of the activator and the inhibitor and are determined by the local kinetic coefficients: the relaxation times and the diffusion coefficients  $D_\theta$  and  $D_\eta$ . In real systems these kinetic coefficients strongly depend on the excitation level of the system and the state of the environment, the presence of small amounts of impurities or catalysts which, for example, may change the rates of recombination of nonequilibrium carriers in semiconductors or the rates of chemical reactions, and so on. For example, by varying only the temperature of the semiconductor lattice, one can significantly change the critical parameters of the electron-hole plasma described by Eqs. (3) and (4) [27].

We have shown that by changing the values of  $\epsilon$  and  $\alpha$  and the control parameter  $A$  (in the physical systems, such as electron-hole plasma,  $A$  is the system's excitation level), that is, in essentially the same system the whole variety of domain patterns and pattern formation scenarios is realized. This general conclusion explains theoretically the results of recent experiments by Lee *et al.* on the FIS reaction [15–17] where they showed that in this chemical system by changing relatively weakly its chemical composition and the form of the initial perturbation it is possible to excite all major types of domain patterns and see various scenarios of their formation, which are qualitatively the same as those observed in our simulations.

In KN systems, that is, when  $\epsilon \ll 1$  and  $\alpha \gg \epsilon$  only static patterns form. When the homogeneous state of the KN system is stable, these patterns can be excited by applying a sufficiently strong perturbation (hard excitation). We found that by changing only the parameter

$A$  and the form of the initial perturbation one can excite localized spots and stripes, connected (Fig. 5) and disconnected (Fig. 6) labyrinthine patterns, wriggled stripes (Fig. 7) and multidomain patterns (Fig. 3). All these patterns were found in the chemical experiments [6,8,17]. Ordered multidomain patterns were also observed in the high frequency gas-discharge experiments [19] and in the combustion experiments [20]. We also found that at the same parameters of the KN system it is possible to excite a great variety of shapes of the static patterns by changing only the form of the initial perturbation. In particular, it is possible to excite the labyrinthine and multidomain patterns in the system with the same values of the parameters  $\epsilon$ ,  $\alpha$ , and  $A$  [33]. This variety of domain shapes is observed when  $\epsilon$  is not very small, since for very small values of  $\epsilon$  only disconnected multidomain patterns will form [33]. However, such small values of  $\epsilon$  can hardly be realized in a typical experimental situation. That's why in our paper we paid particular attention to the case  $\epsilon = 0.05$ .

Static domain patterns in KN systems may also form spontaneously as a result of Turing instability of the homogeneous state. In the ideally homogeneous KN systems these patterns are as a rule quasiperiodic (Fig. 3) and in general their period is not the same as the period of the critical fluctuation  $2\pi/k_0$  [see Eq. (12)], but is determined by the stability of the pattern. In real systems the type of the pattern will be determined by the small local inhomogeneities. Depending on the form of the inhomogeneity, and also on the system's parameters, all types of static domain patterns will form spontaneously in KN systems.

In  $\Omega N$  systems, that is when  $\alpha \ll 1$  and  $\alpha \lesssim \epsilon^2$ , only the uniform relaxation self-oscillations may form spontaneously. In such systems with the stable homogeneous state various autowave patterns, including expanding traveling waves [Fig. 13(a)] and spiral waves, can be excited by an external perturbation. If the initial conditions are sufficiently random, the spiral turbulence [Fig. 13(b)] forms in  $\Omega N$  systems. These patterns were first discovered by Zaikin and Zhabotinsky in an oscillatory chemical reaction [39] and have been subsequently studied for more than two decades in a variety of systems [2,3,5,8]. Notice that the autowave patterns are also observed in the FIS reaction [17].

The most diverse picture of pattern formation is observed in the case of  $K\Omega N$  systems, that is, when  $\epsilon \ll 1$  and  $\epsilon^2 \lesssim \alpha \lesssim \epsilon$ . In these systems both the uniform self-oscillations and the Turing patterns may form spontaneously. In the  $K\Omega N$  systems with the stable homogeneous state it is possible to excite static, traveling, and pulsating (breathing) patterns. We showed that in these systems the remarkable effect of self-replication of spots (Figs. 8 and 10) recently discovered in the same FIS reaction [16,17] is realized. Depending on the system's parameters, this process may lead to the formation of static or pulsating multidomain pattern, or to the formation of turbulence which is qualitatively different from

the spiral turbulence observed in  $\Omega N$  systems. This turbulence consists of random creation and annihilation of spots. Precisely this kind of turbulence was observed in the experiments in the very same FIS reaction [17], and also in the combustion experiments [22].

We would like to emphasize that the whole variety of pattern formation scenarios observed in our numerical simulations and illustrated in Fig. 15 is explained with the remarkable accuracy by the asymptotic theory of instabilities of domain patterns in reaction-diffusion systems [23]. This is because the scenarios of pattern formation are determined by the two processes: at first any initial perturbation quickly transforms to a state close to some stationary state, then the evolution of that quasistationary state is determined by its instabilities and the form of the critical fluctuations with respect to which the instability is realized. Indeed, the stationary states correspond to the solutions of Eqs. (1) and (2) with the right-hand sides equal to zero, so when we use the initial conditions which are significantly different from any stationary state, we in fact make the right-hand sides of Eqs. (1) and (2) large and, therefore, the time derivatives of  $\theta$  and  $\eta$ . The large time derivatives will cause such changes in  $\theta$  and  $\eta$  which will lead to the transformation of the initial condition to the state close to some stationary state, in which the time derivatives of  $\theta$  and  $\eta$  are small. For example, if a square of relatively small size is used as the initial condition, it will first transform to a state close to a spot; if a square of large size ( $\gg L$ ) is used, it will first transform into an annulus as a result of the local breakdown in the center of the square (this effect was studied in detail in Refs. [10–12]). If the system is bistable, the initial condition in the form of a large square may trigger the wave of switching from one stable homogeneous state to the other. The evolution of these states close the stationary states, and, therefore, the pattern formation scenarios, will be determined by their stability: a spot may form from a square of small size if the parameters of the system are such that it is stable, or an annulus may form from a square of large size. The radius of the spot, or the width and size of the annulus will be determined by the corresponding stable states and will only depend on the parameters of the system (such as  $\epsilon$  and  $A$ ). If the parameters of the system are such that these states happen to be unstable, then, depending on the type of the instability, which is determined by the parameters  $\epsilon$ ,  $\alpha$ , and  $A$ , all kinds of complex patterns will form.

One of the bright pattern formation scenarios consists of the transformation of the localized excitations into the patterns that fill the entire system. In certain sense one could think of this as the self-completion of a pattern from its small fragment. According to Figs. 3 – 7, the form of such patterns depends on both the initial conditions and the integral parameters of the system (in our case  $\epsilon$ ,  $\alpha$ , and  $A$ ) which are determined by the system's kinetics. It is important that by changing only these integral parameters it is possible to excite qualitatively different patterns for the same initial condition. Thus,

the systems we consider have a remarkable property — a kind of associative memory (see also Refs. [11,12]): the form of a pattern is determined by the integral parameters of the *ideally homogeneous system*, and they can be reconstructed with certain probability from a small fragment (sufficiently localized initial perturbation).

Patterns of the same morphology as those in the KN system studied by us also form in a variety of the equilibrium systems, such as garnet ferromagnets, ferroelectric and ferrofluid films, Langmuir monolayers, phase-separating copolymer blends (for a recent review and the references see Ref. [18]). Our simulations suggest that the complex domain patterns, such as multidomain or labyrinthine patterns, are driven by the dynamics of their interfaces coupled to the long-ranged inhibitor field. It is, therefore, natural to expect qualitatively the same pattern formation scenarios in the equilibrium systems with the competing repulsive interactions and the strong separation of length scales. In the nonequilibrium systems the inhibitor does not necessarily react on the motion of the pattern interfaces instantaneously. The time lag of the inhibitor makes the existence of complex dynamic patterns possible in the nonequilibrium systems.

The only kinds of patterns that form in the experiments with the cellular flames [21] and with the gas-discharge system [19] we did not see in our numerical simulations are traveling spots and hopping patterns. Recent work of Krischer and Mikhailov suggested that a sufficiently strong global coupling, which is absent in our model, might be needed to see these kinds of patterns [40].

- 
- [1] G. Nicolis and I. Prigogine, *Self-organization in Non-Equilibrium Systems* (Wiley Interscience, New York, 1977).
  - [2] *Oscillating and Traveling Waves in Chemical Systems*, edited by R. J. Field and M. Burger (Wiley Interscience, New York, 1985).
  - [3] V. A. Vasiliev, Y. M. Romanovskii, D. S. Chernavskii, and V. G. Yakhno, *Autowave Processes in Kinetic Systems: Spatial and Temporal Self-Organization in Physics, Chemistry, Biology, and Medicine* (VEB Deutscher Verlag der Wissenschaften, Berlin, 1987).
  - [4] J. D. Murray, *Mathematical Biology* (Springer-Verlag, Berlin, 1989).
  - [5] A. S. Mikhailov, *Foundations of Synergetics* (Springer-Verlag, Berlin, 1990).
  - [6] I. Lengyel and I. R. Epstein, *Acc. Chem. Res.* **26**, 235 (1993).
  - [7] M. Cross and P. C. Hohenberg, *Rev. Mod. Phys.* **65**, 851 (1993).
  - [8] *Chemical waves and patterns*, edited by R. Kapral and K. Showalter (Kluwer, Dordrecht, 1995).
  - [9] B. S. Kerner and V. V. Osipov, in *Self-organization by*

*nonlinear irreversible processes*, edited by W. Ebeling and H. Ulbricht (Springer, New York, 1986).

- [10] B. S. Kerner and V. V. Osipov, *Sov. Phys. – Uspekhi* **33**, 679 (1990).
- [11] B. S. Kerner and V. V. Osipov, *Sov. Phys. – Uspekhi* **32**, 101 (1989).
- [12] B. S. Kerner and V. V. Osipov, *Autosolitons: a New Approach to Problems of Self-Organization and Turbulence* (Kluwer, Dordrecht, 1994).
- [13] *Nonlinear dynamics and pattern formation in semiconductors and devices*, edited by F. J. Niedernostheide (Springer, Berlin, 1994).
- [14] M. Bode and H.-G. Purwins, *Physica D* **86**, 53 (1995).
- [15] K. J. Lee, W. D. McCormick, Q. Ouyoung, and H. L. Swinney, *Science* **261**, 189 (1993).
- [16] K. J. Lee, W. D. McCormick, Q. Ouyoung, and H. L. Swinney, *Letters to Nature* **369**, 215 (1994).
- [17] K. Lee and H. Swinney, *Phys. Rev. E* **51**, 1899 (1995).
- [18] M. Seul and D. Andelman, *Science* **267**, 476 (1995).
- [19] E. Ammelt, D. Schweng, and H.-G. Purwins, *Phys. Lett. A* **179**, 348 (1993).
- [20] M. Gorman, M. el Hamdi, and K. A. Robbins, *Combust. Sci. Tech.* **98**, 37 (1994).
- [21] M. Gorman, M. el Hamdi, and K. A. Robbins, *Combust. Sci. Tech.* **98**, 71 (1994).
- [22] M. Gorman, M. el Hamdi, and K. A. Robbins, *Combust. Sci. Tech.* **98**, 79 (1994).
- [23] C. B. Muratov and V. V. Osipov, *Phys. Rev. E* **53**, 3101 (1996).
- [24] T. Ohta and K. Kawasaki, *Macromolecules* **19**, 2621 (1986).
- [25] T. Ohta, A. Ito, and A. Tetsuka, *Phys. Rev. A* **42**, 3225 (1990).
- [26] R. F. Mamin, *JETP Lett.* **60**, 52 (1994).
- [27] B. S. Kerner and V. V. Osipov, *Sov. Phys. – JETP* **62**, 337 (1985).
- [28] P. Ortoleva and J. Ross, *J. Chem. Phys.* **63**, 3398 (1975).
- [29] R. C. Casten, H. Cohen, and P. A. Lagerstrom, *Quart. Appl. Math.* **32**, 365 (1975).
- [30] T. Ohta, M. Mimura, and R. Kobayashi, *Physica D* **34**, 115 (1989).
- [31] A. Hagberg and E. Meron, *Phys. Rev. Lett.* **72**, 2494 (1994).
- [32] R. E. Goldstein, D. J. Muraki, and D. M. Petrich, *Phys. Rev. E* **53**, 3933 (1996).
- [33] C. B. Muratov, *Phys. Rev. E* (to be published).
- [34] P. C. Fife, *J. Chem. Phys.* **64**, 554 (1976).
- [35] A. Hagberg and E. Meron, *Chaos* **4**, 477 (1994).
- [36] D. Haim *et al.*, *Phys. Rev. Lett.* **77**, 190 (1996).
- [37] V. V. Osipov, I. I. Lazurchak, B. S. Kerner, and V. V. Gafichuk, *Mikroelektronika* **16**, 23 (1987).
- [38] V. V. Osipov, *Physica D* **93**, 143 (1996).
- [39] A. N. Zaikin and A. M. Zhabotinsky, *Nature* **225**, 535 (1970).
- [40] K. Krischer and A. Mikhailiov, *Phys. Rev. Lett.* **73**, 3163 (1994).

FIG. 1. The nullclines of Eqs. (5) and (6).

FIG. 2. The simplest domain patterns: (a) traveling, (b) static, (c) pulsating one-dimensional autosolitons.

FIG. 3. Formation of static Turing pattern. The distributions of the activator at times. The parameters used:  $\epsilon = 0.05$ ,  $\alpha = 0.5$ ,  $A = -0.1$ . The system's size is  $20 \times 20$ .

FIG. 4. Formation of static Turing pattern in an oscillatory system. The distributions of the activator at different times. The parameters used:  $\epsilon = 0.05$ ,  $\alpha = 0.05$ ,  $A = -0.1$ . The system's size is  $20 \times 20$ .

FIG. 5. Formation of a connected labyrinthine pattern. The distributions of the activator at different times. The parameters used:  $\epsilon = 0.05$ ,  $\alpha = 0.2$ ,  $A = -0.4$ . The system's size is  $20 \times 20$ .

FIG. 6. Formation of a disconnected labyrinthine pattern. The distributions of the activator at different times. The parameters used:  $\epsilon = 0.05$ ,  $\alpha = 0.2$ ,  $A = -0.25$ . The system's size is  $20 \times 20$ .

FIG. 7. Formation of a wriggled stripe. The distributions of the activator at different times. The parameters used:  $\epsilon = 0.05$ ,  $\alpha = 0.2$ ,  $A = -0.45$ . The system's size is  $20 \times 20$ .

FIG. 8. Self-replicating spots. The distributions of the activator at different times. The parameters used:  $\epsilon = 0.05$ ,  $\alpha = 0.015$ ,  $A = -0.4$ . The system's size is  $20 \times 20$ .

FIG. 9. The value of  $\eta$  in the center of the system as a function of time in the simulation with  $\epsilon = 0.05$ ,  $\alpha = 0.015$ ,  $A = -0.3$  which resulted in the pulsating multidomain pattern. The system's size is  $10 \times 10$ .

FIG. 10. A close-up of a self-replicating spot. Same simulation as in Fig. (8). The region shown is  $8 \times 8$ .

FIG. 11. The onset of turbulence. The distributions of the activator at different times. The parameters used:  $\epsilon = 0.05$ ,  $\alpha = 0.01$ ,  $A = -0.4$ . The system's size is  $10 \times 10$ .

FIG. 12. The value of  $\eta$  in the center of the system as a function of time for the simulation of Fig. 11.

FIG. 13. The distributions of the activator at different times for different processes: (a) formation of an autowave ( $\epsilon = 0.05, \alpha = 0.007, A = -0.3$ , the system is  $20 \times 20$ ); (b) formation of spiral turbulence ( $\epsilon = 0.25, \alpha = 0.02, A = -0.3$ , the system is  $100 \times 100$ ); (c) stabilization of a pattern formed in the process of splitting of spots ( $\epsilon = 0.05, \alpha = 0.02, A = -0.3$  the system is  $10 \times 10$ ); (d) formation of a complex pattern outside the asymptotic regime ( $\epsilon = 0.2, \alpha = 1.0, A = -0.15$ , the system's size is  $40 \times 40$ ).

FIG. 14. The dependences of  $\mathcal{L}_s$  on  $A$  for the one-dimensional AS (a) and  $\mathcal{R}_s$  on  $A$  for the radially-symmetric AS (b) for  $\epsilon = 0.05$ . Results of the numerical simulations of Eqs. (7) and (8).

FIG. 15. The domains of existence of different patterns at  $\epsilon = 0.05$ . The upper part of the figure shows the regions where the corresponding patterns may exist at  $\alpha \gg \epsilon$ . The lower-case letters indicate the long-time behavior of the system at the parameters corresponding to the position of the letter when the system is locally excited at  $t = 0$ : “s” — the system aperiodically relaxes to a static pattern; “ps” — the system relaxes to a static pattern, but the relaxation has oscillating character, a few splittings may occur at the beginning; “p” — as a result of self-replications at the beginning a stationary pulsating (breathing) pattern forms in the system; “c” — the initial excitation collapses as a result of the growing amplitude of pulsations; “t” — turbulence develops in the system; “a” — the initial excitation transforms into an autowave traveling through the system and disappearing at the boundaries. The upper dashed line shows schematically the region where the character of pattern's relaxation changes from aperiodic to oscillating. The upper solid line is the threshold of the instability with respect to the uniform pulsations for a radially symmetric AS, obtained from Eq. (17). The lower solid line is the threshold of the instability leading to the transformation of the radially symmetric AS into traveling, obtained from Eq. (17). The lower dashed lines show schematically the borders of the parameter regions where pulsating patterns or turbulence are realized.

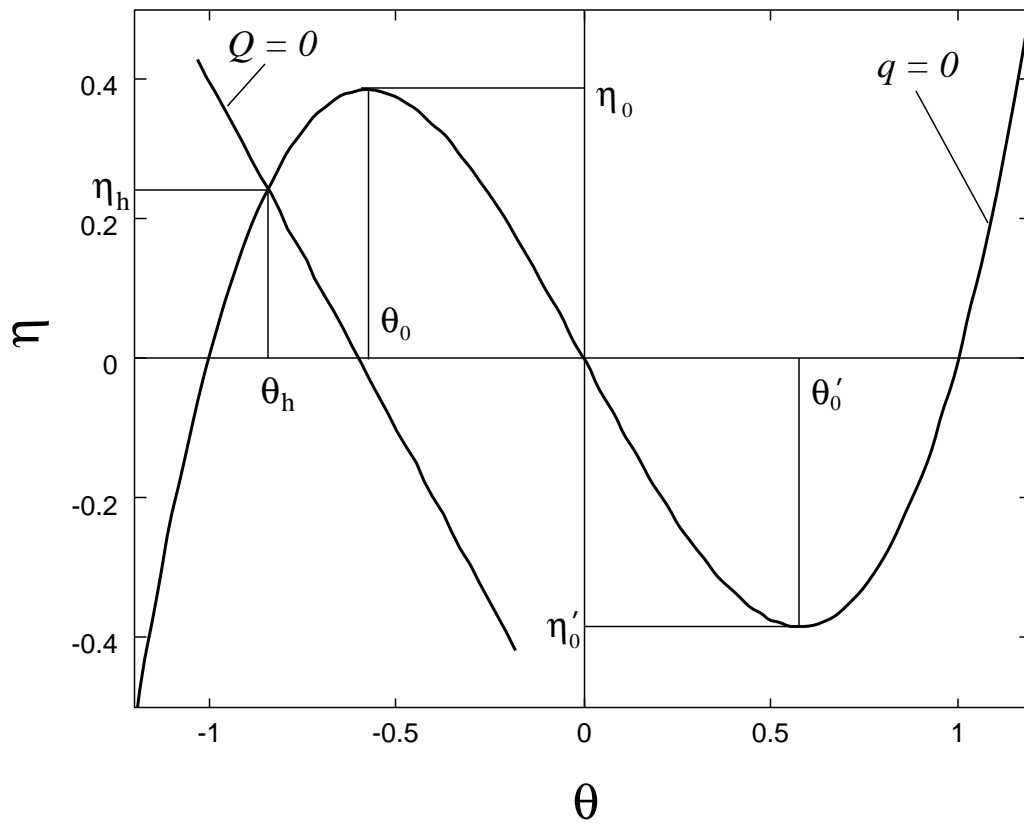


Fig. 1

Muratov



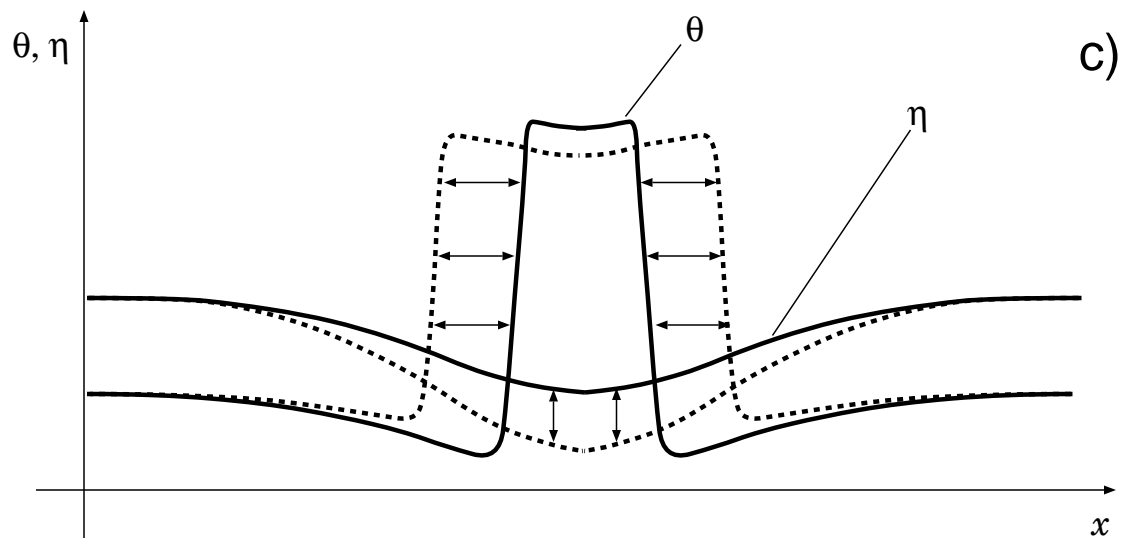
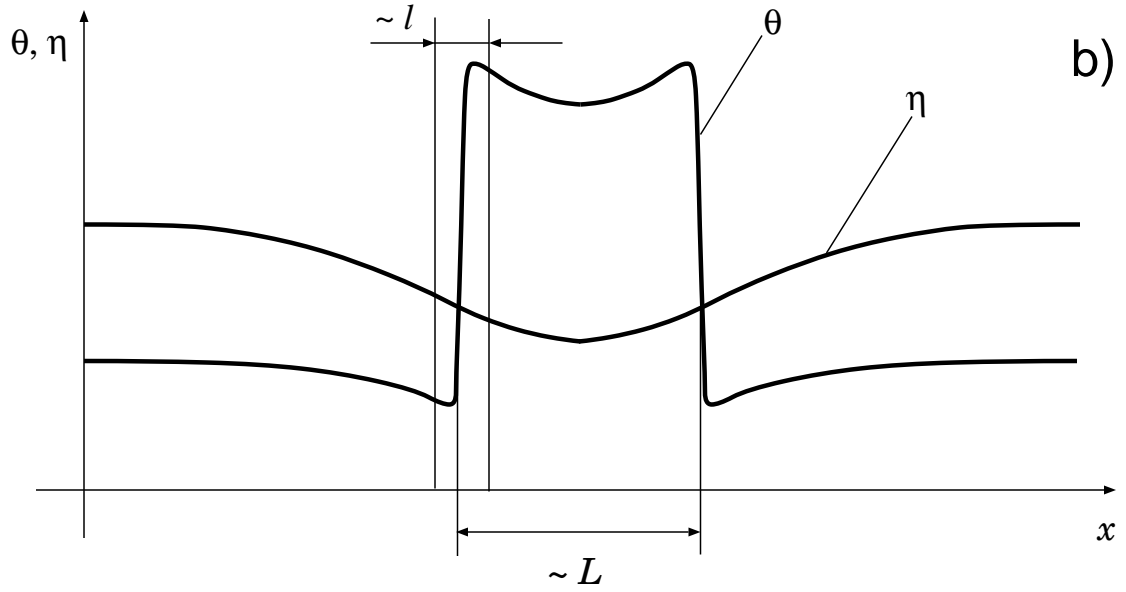
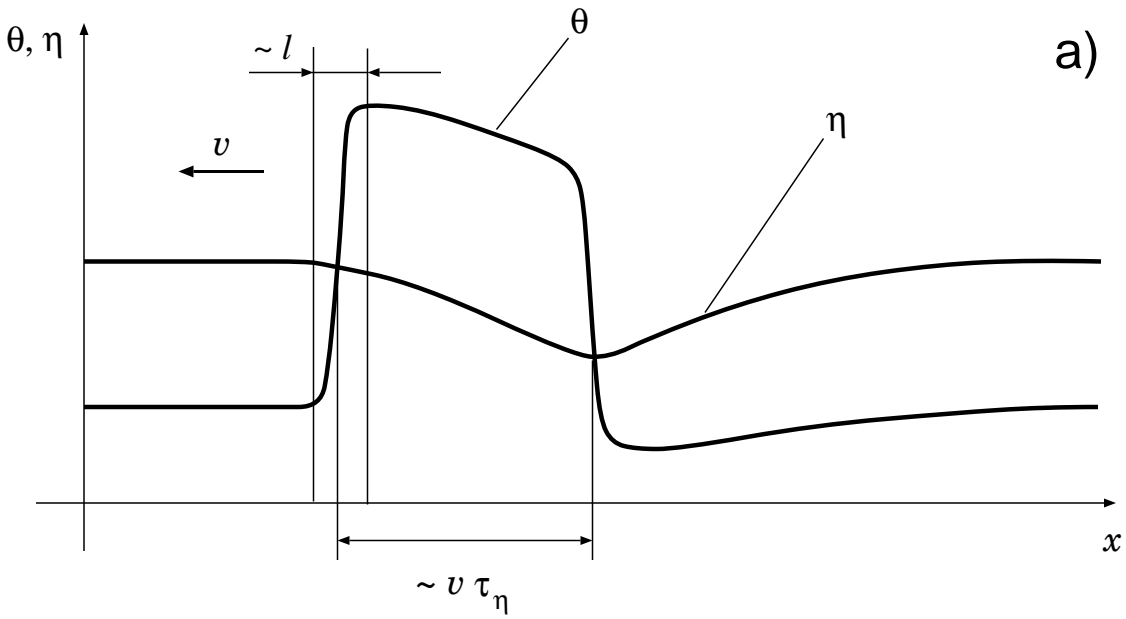


Fig. 2

Muratov

This figure "fig3.gif" is available in "gif" format from:

<http://arxiv.org/ps/patt-sol/9607002v1>

This figure "fig4.gif" is available in "gif" format from:

<http://arxiv.org/ps/patt-sol/9607002v1>

This figure "fig5.gif" is available in "gif" format from:

<http://arxiv.org/ps/patt-sol/9607002v1>

This figure "fig6.gif" is available in "gif" format from:

<http://arxiv.org/ps/patt-sol/9607002v1>

This figure "fig7.gif" is available in "gif" format from:

<http://arxiv.org/ps/patt-sol/9607002v1>

This figure "fig8.gif" is available in "gif" format from:

<http://arxiv.org/ps/patt-sol/9607002v1>

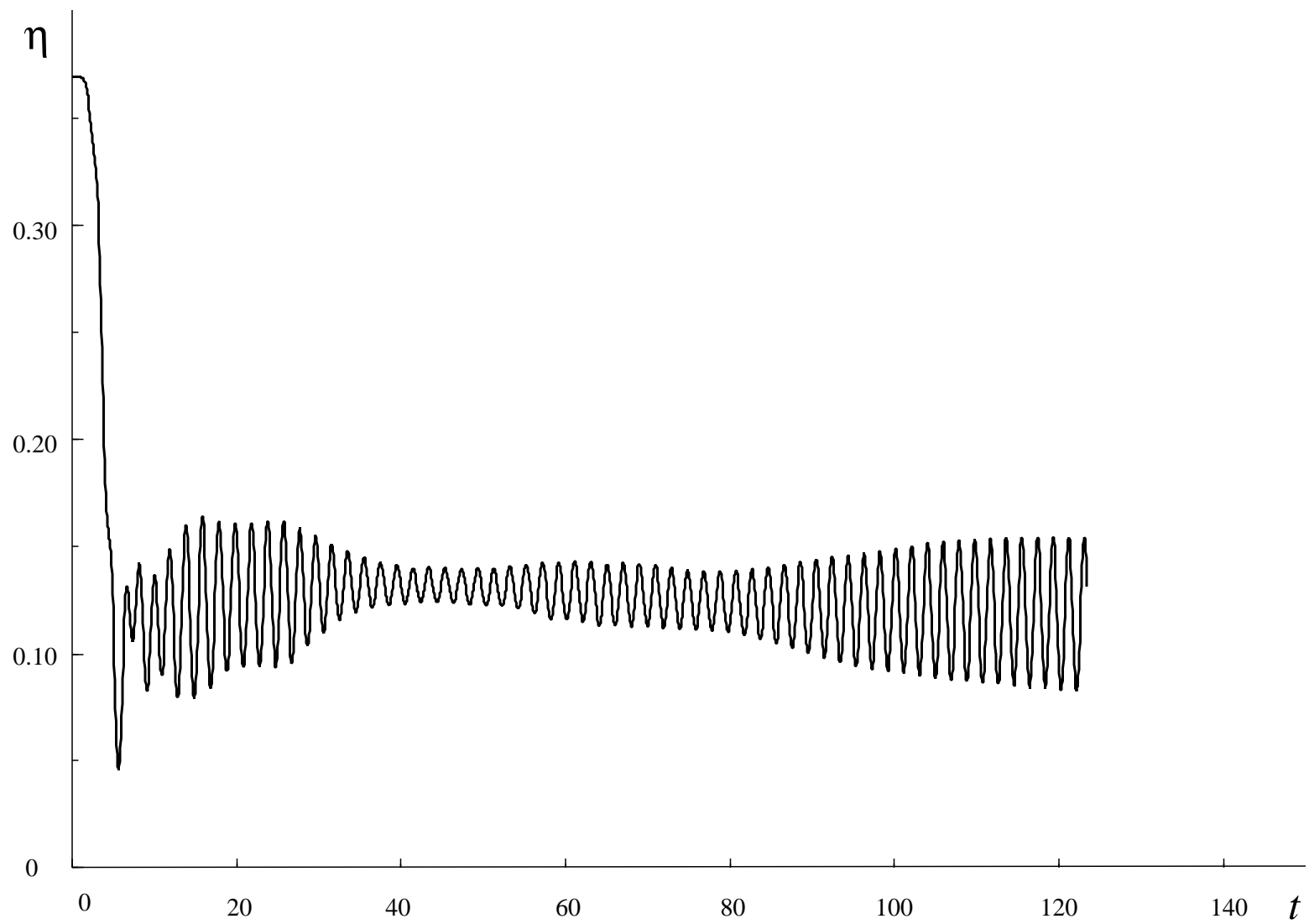
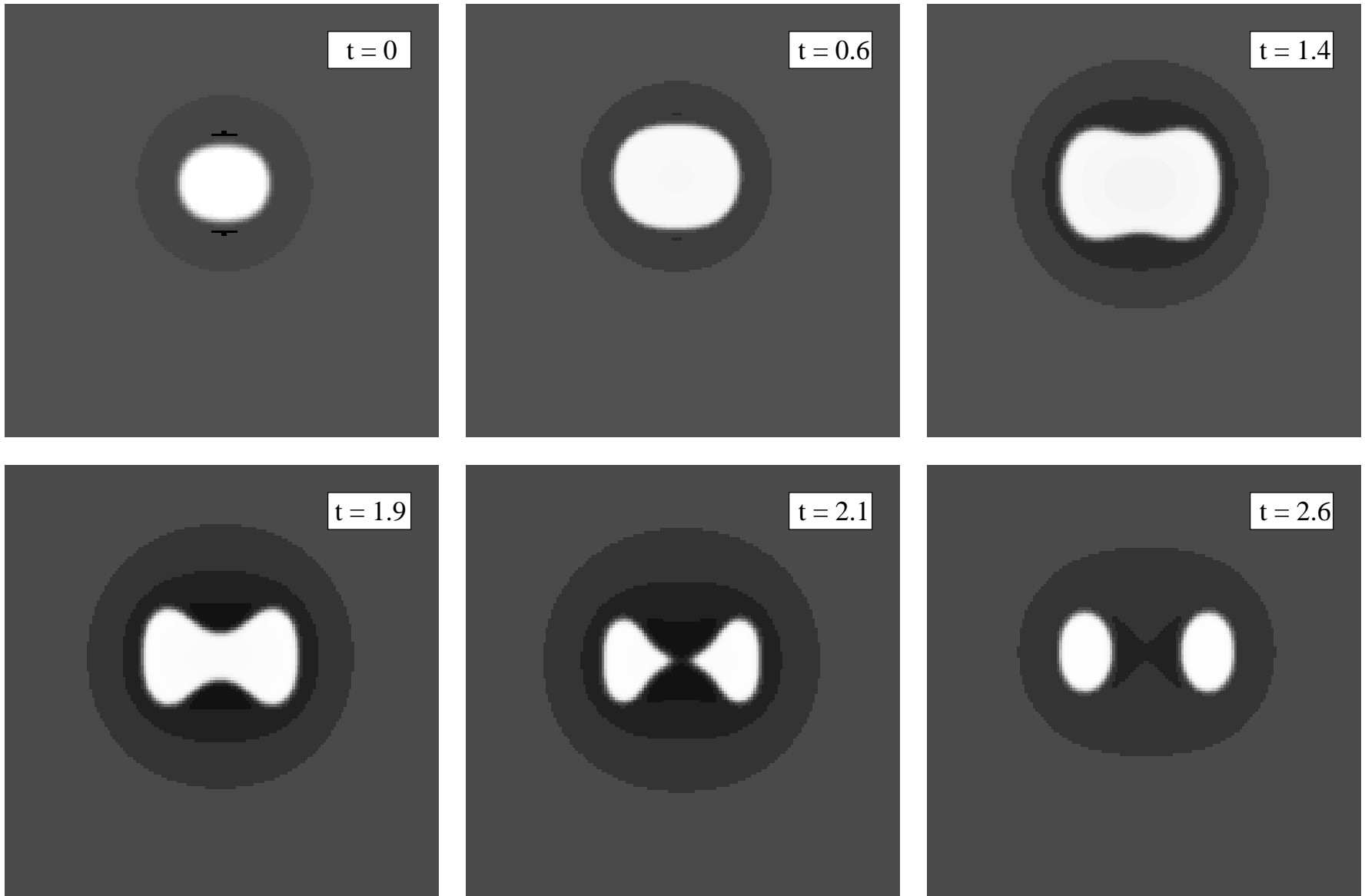


Fig. 9

Muratov





Muratov

Fig.10

This figure "fig11.gif" is available in "gif" format from:

<http://arxiv.org/ps/patt-sol/9607002v1>

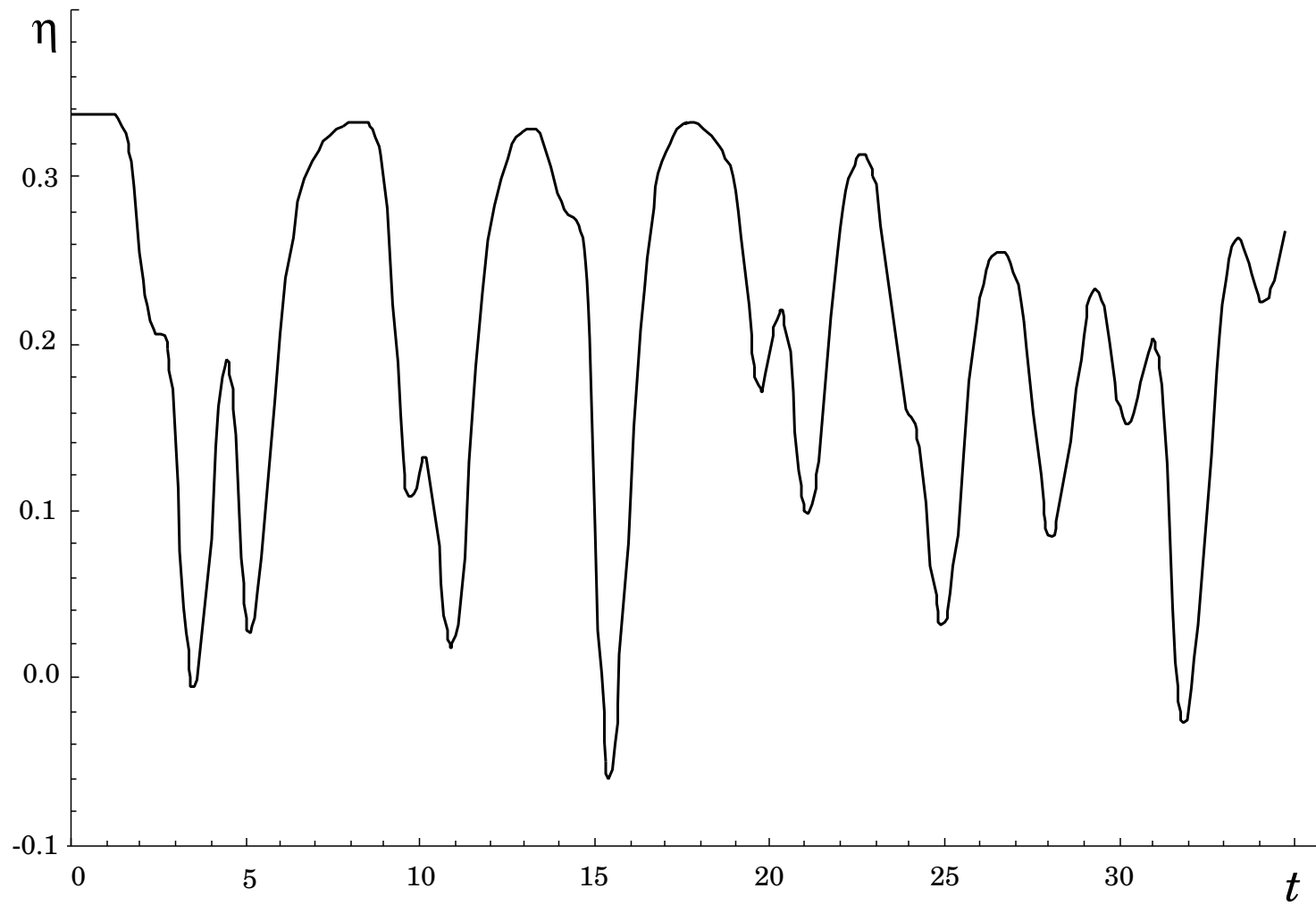


Fig. 12

Muratov

This figure "fig13a.gif" is available in "gif" format from:

<http://arxiv.org/ps/patt-sol/9607002v1>

This figure "fig13b.gif" is available in "gif" format from:

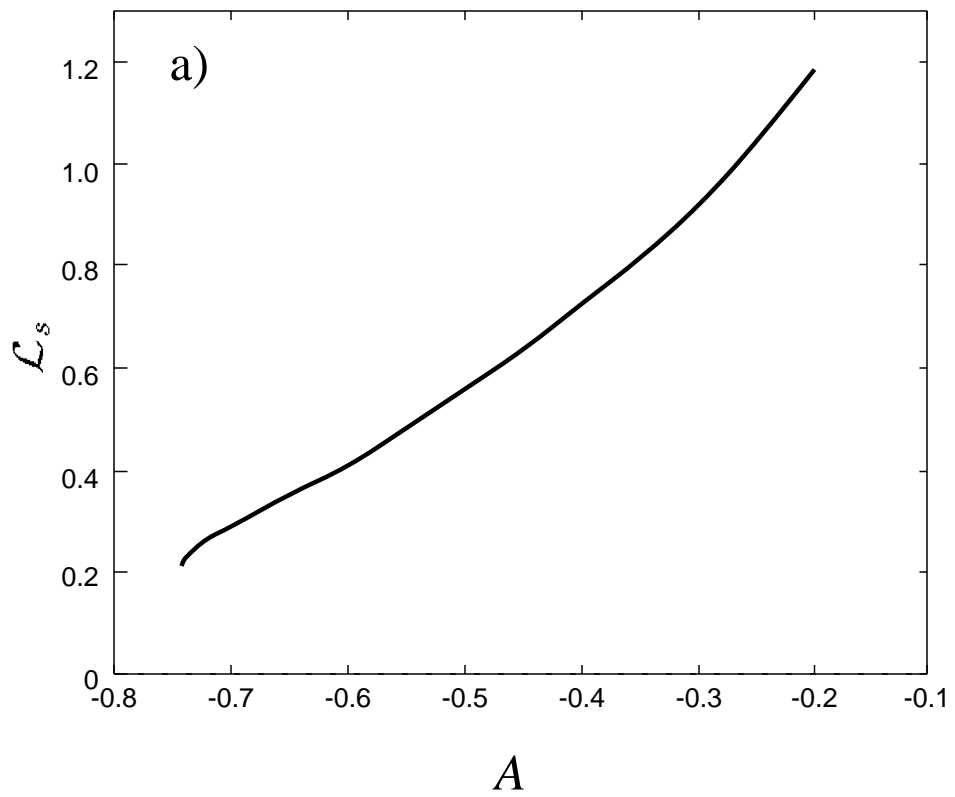
<http://arxiv.org/ps/patt-sol/9607002v1>

This figure "fig13c.gif" is available in "gif" format from:

<http://arxiv.org/ps/patt-sol/9607002v1>

This figure "fig13d.gif" is available in "gif" format from:

<http://arxiv.org/ps/patt-sol/9607002v1>



Muratov

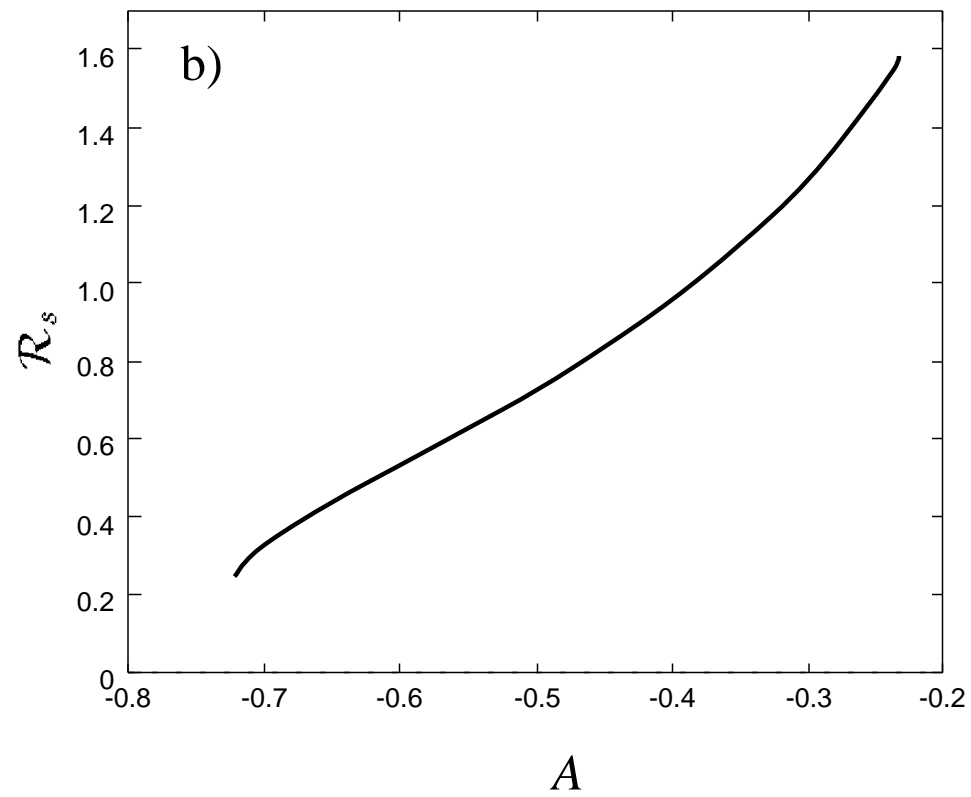


Fig. 14



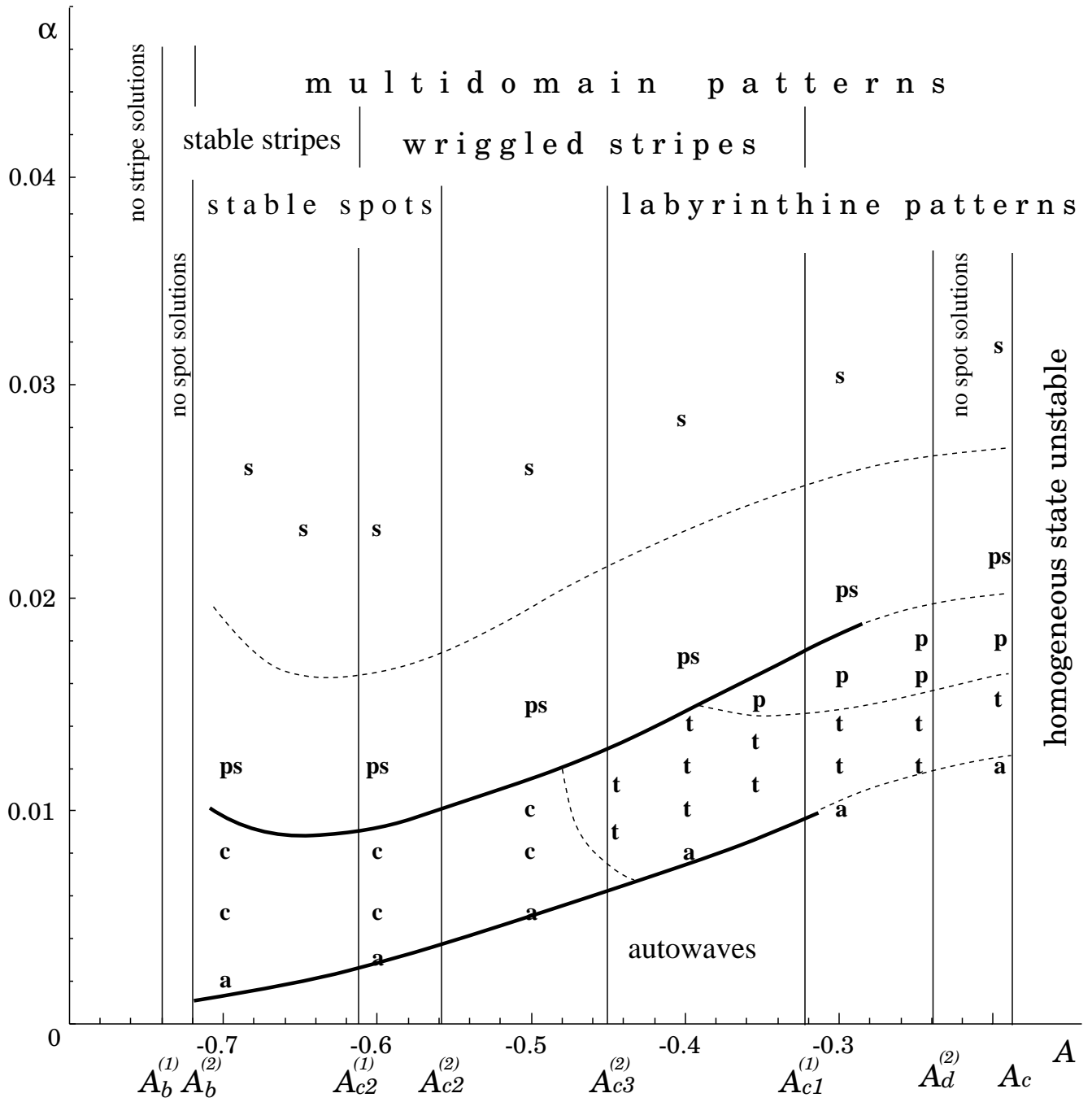


Fig. 15

Muratov